AO

PCT

WORLD INTELLECTUAL PROPERT
International Bure:

WO   9607161A1

INTERNATIONAL APPLICATION PUBLISHED UNDER T

(51) International Patent Classification ^{6} :		(11) International Publication Number:	**WO 96/07161**
G06T 7/00	**A1**	(43) International Publication Date:	7 March 1996 (07.03.96)

(21) International Application Number: PCT/DK95/00338

(22) International Filing Date: 21 August 1995 (21.08.95)

(30) Priority Data:
0996/94   29 August 1994 (29.08.94)   DK
0578/95   19 May 1995 (19.05.95)   DK

(71) Applicant *(for all designated States except US)*: ESKOFOT A/S [DK/DK]; Industriparken 35-37, DK-2750 Ballerup (DK).

(72) Inventors; and
(75) Inventors/Applicants *(for US only)*:   GRUNKIN, Michael [DK/DK]; Frederiksborgvej 105, 4. th., DK-2400 Copenhagen NV (DK). FREDFELDT, Knud, Erik [DK/DK]; Gondolvej 45, DK-4040 Jyllinge (DK). HYLDSTRUP, Lars [DK/DK]; Maglevanget 9, DK-2920 Charlottenlund (DK). CONRADSEN, Knut [DK/DK]; Søndervangen 76, DK-3460 Birkerød (DK).

(74) Agent: PLOUGMANN & VINGTOFT A/S; Sankt Annæ Plads 11, P.O. Box 3007, DK-1021 Copenhagen K (DK).

(81) Designated States: AM, AT, AT (Utility model), AU, BB, BG, BR, BY, CA, CH, CN, CZ, CZ (Utility model), DE, DE (Utility model), DK, DK (Utility model), EE, EE (Utility model), ES, FI, FI (Utility model), GB, GE, HU, IS, JP, KE, KG, KP, KR, KZ, LK, LR, LT, LU, LV, MD, MG, MK, MN, MW, MX, NO, NZ, PL, PT, RO, RU, SD, SE, SG, SI, SK, SK (Utility model), TJ, TM, TT, UA, UG, US, UZ, VN, European patent (AT, BE, CH, DE, DK, ES, FR, GB, GR, IE, IT, LU, MC, NL, PT, SE), OAPI patent (BF, BJ, CF, CG, CI, CM, GA, GN, ML, MR, NE, SN, TD, TG), ARIPO patent (KE, MW, SD, SZ, UG).

Published
With international search report.
With amended claims.

(54) Title: A METHOD OF ESTIMATION
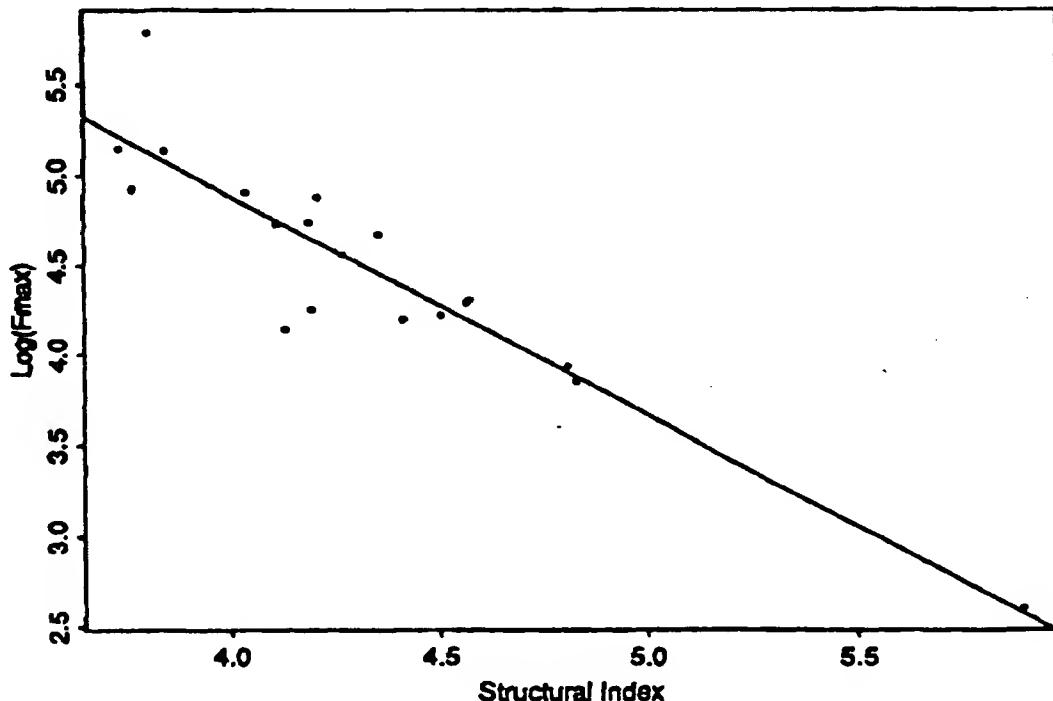
(57) Abstract

A method is described for estimating the bone quality of a vertebrate, on the basis of two-dimensional image data comprising information relating to the trabecular structure of at least a part of a bone of the vertebrate, the image data being data obtained by exposing at least the part of the bone to electromagnetic radiation, the method comprising subjecting the image data to a statistical analysis.

A METHOD OF ESTIMATION

The present invention relates to the field of non-invasive
determination of bone quality of vertebrates. This determina-
tion may be used in the diagnosis of, e.g., osteoporosis and
5   other bone diseases which cause bone fragility and, thus,
increase the risk of bone fracture.

Accelerated bone loss leading to osteoporosis is a common
phenomenon in women after menopause. Women often ignorantly
suffer from accelerated bone loss, and the reduced strength
10 of the bones is not discovered until a bone is broken or a
vertebra collapses due to a load which a healthy bone or
vertebra should be able to withstand. Thus, a large part of
the osteoporotic patients are not aware of the reduced
strength of their bones until a fracture reveals the disease
15 and the extent thereof.

Today, osteoporosis affects more than one third of elderly
women in the industrialized part of the world. The prevalence
of this disease is still increasing, partly caused by the
increase in the proportion of elderly people, partly for
20 unexplained reasons. In the lesser developed parts of the
world, like South-east Asia and South America, it is pre-
dicted that osteoporosis will become an enormous socio-econo-
mic burden within the next 20-30 years. However, if indivi-
duals at risk of developing osteoporosis can be identified,
25 preventive measures can be applied. This requires a reliable,
cheap and safe method for identification of those at risk.

Since the risk of osteoporosis is closely related to the bone
resistance to fracture, bone strength or bone quality mea-
surements are likely to supply the essential information.

30 Since the means of preventing osteoporosis are much more
efficient than those of treating osteoporosis, identification
of individuals at risk of developing this disease is crucial.
Only by early prevention of osteoporosis, the individual as

well as the socio-economic consequences of the disease may be minimized.

The method according to the invention provides a method for detection of reductions in bone quality, such as architecture
5   and strength, at an early stage. Thus, the method of the invention provides a tool of screening potential patients for bone diseases and, thus, provides the possibility of early detection of bone diseases at a stage in which no symptoms of disease are noted by the patient.

10 A typical measure of bone strength has been the Bone Mineral Density (BMD) of the bone. BMD measurements are typically obtained by X-ray of a bone together with a standard wedge. Having determined which part of the wedge attenuates the X-ray beam to the same degree as the illuminated bone, a
15 measure of BMD may be obtained.

A more sophisticated method of determining BMD is by X-ray absorptiometry of two different wavelengths. Using two wavelengths enables the method to compensate for the effects of soft tissue etc. around the bone and, thus, to obtain a more
20 exact determination of the X-ray attenuation of the bone.

However, as will be clear from the following, the Bone Mineral Density of a bone is not necessarily connected to the actual strength of the bone. The reason for this is to be found in the structure of a bone of a vertebrate.

25 A bone of a vertebrate consists of a cortical outer layer and a cancellous inner structure. Omission of the cancellous inner structure of a bone would result in a quite fragile bone. The cancellous inner structure of the bone consists of so-called trabeculae. Thicker vertical trabeculae are
30 positioned in the bone in the direction of the main load (main compression or pull in the bone), and thinner, horizontal trabeculae interconnect the vertical trabeculae.

Thus, the main density of a bone is constituted by the corti-
cal layer and the vertical trabeculae. This is quite natural,
as the bone reserves the largest part of the material to
withstand the most common loads. A BMD measurement
5   determining the density of a bone will therefore primarily
estimate the amount of bone in the cortical layer and the
vertical trabeculae and, thus, only to some degree the
ability of the bone to withstand the loads to which the bone
is adapted.

10 However, when loads are applied not in the direction of the
vertical trabeculae, the structure of the bone would be
fragile without the thinner, horizontal trabeculae which
interconnect the vertical trabeculae. The horizontal
trabeculae define the ability of the bone to withstand loads
15 not in the direction of the vertical trabeculae. Thus, the
strength of the bone in directions not in the direction of
the vertical trabeculae is defined by a very small part of
the bone mass.

Different bones vary in the relation between cortical and
20 trabecular bone structures. Furthermore, the architecture of
the trabeculae vary according to the potential loading of
this part of the bone. The number and diameter of
longitudinal trabeculae and the presence of transverse
trabeculae are also of fundamental importance for the
25 fragility of the bone. These differences are of major
importance for the strength of the bone, but they can only to
a minor extent be detected by BMD measurements.

Since trabecular bone has a greater surface area/weight
ratio, it is to a higher extend exposed to accelerated bone
30 loss than the cortical bone. Therefore, osteoporotic frac-
tures are mainly seen in bones with predominantly trabecular
structure, such as the distal forearm, proximal humerus,
thoracic and lumbar spine as well as the femoral neck.
Changes in BMD related to loss of trabecular bone severely
35 underestimates the loss of resistance to fracture. As a

consequence, BMD measurements of patients with osteoporotic
fractures reveal a major overlap with BMD measurements of
normal subjects of the same cohort.

The above information explains why persons with low energy
5   fractures may have normal BMD values when compared to age-
matched normal controls. Thus, one may wish to distinguish
between bone quantity and bone quality, where the bone qual-
ity is more closely related to the mechanical or bio-mechan-
ical strength of the bone.

10   A measure of the overall bone strength may naturally be
obtained from a bone specimen taken from the potential
patient and subjected to mechanical testing. However, this
requires bone biopsy, which is painful and implies a minor
risk of complications. Thus, in order to have a comfortable,
15   cheap, fast and safe screening of the very large group of
potential patients (most women after menopause), the estima-
tion of the bone quality should be performed non-invasively
in a safe and fast manner.

The present invention offers a non-invasive method which
20   provides measures of the overall strength of bones and which
is safe, comfortable for the potential patient, fast and
cheap.

In "A New Method for Automatic Recognition of the Radio-
graphic Trabecular Pattern" Wil G.M. Geraets et al., Journal
25   of Bone and Mineral Research, Vol. 5, No. 3, 1990, pp 227-
233, a method of recognizing the trabecular pattern from X-
ray pictures is disclosed. According to this method, two
types of noise are removed from an X-ray picture which has
been scanned into an image memory: high-frequency noise is
30   removed by using a median filter, and low-frequency noise is
removed by using a local averaging operation on the image.

After noise reduction a segmentation of the image data is
performed whereby the image is binarized and subsequently

eroded (by using a median axis transform) so as to retain
only central lines having a thickness of 1 pixel. A total of
7 features are derived from the segmented and the eroded
images. These features are subsequently correlated to the
5   Bone Mineral Density measurements of the bones.

However, due to the almost insignificant correlation between
the image features obtained and the BMD measurements in the
above-mentioned reference, it is evident that a higher cor-
relation and, thus, a more precise estimate of the bone
10   quality is required.

In "computerized Radiographic Analysis of Osteoporosis:
Preliminary Evaluation", Plilip Caligiuri et al, Radiology
1993, 186;417-474, a method in which X-ray images of the
lumbar spine are scanned analyzed. In this reference, the
15   power spectrum was obtained and the Root Mean Square (RMS)
and the First Moment (FMO) thereof were compared to typical
BMD measurements performed on the bones. It was concluded
that both BMD did not correlate well with FMO and RMS and
that this may be due to FMO and RMS containing additional
20   information. In this reference, only the power spectrum and
features derivable therefrom were investigated.

The present invention provides a method and a system for
providing an easily performed, but highly reliable estimation
of the bone quality.

25   In a first aspect, the present invention relates to a method
for estimating the bone quality of a vertebrate, on the basis
of two-dimensional image data comprising information relating
to the trabecular structure of at least a part of a bone of
the vertebrate, the image data being data obtained by expos-
30   ing at least the part of the bone to electromagnetic radi-
ation, the method comprising subjecting the image data to a
statistical analysis comprising

- a background correction procedure in which low frequent intensity variations not related to the trabecular structure of the bone is reduced relative to image data related to the trabecular structure of the part of the bone,

- an image manipulation and feature extraction procedure wherein at least the local image intensity information as well as variation in the local intensity are utilized to extract information related to the trabecular structure of the part of the bone, the image manipulation and feature extraction procedure comprising subjecting the image data to at least one of the following procedures:

    (a)   obtaining an estimate of the parametric estimate of the power spectrum of the image data and extracting features relating to the energy distribution of the parametric estimate,

    (b)   obtaining, on the basis of image data on which a Fourier method has been used to emphasize the information in the image data relating to the trabecular structure, an estimate of a grey-level co-occurrence matrix and extracting at least one feature on the basis of the estimated co-occurrence matrix,

    (c)   obtaining an estimate of the projected trabecular pattern of the image data by using a Fourier method to emphasize the information in the image data relating to the trabecular structure and subjecting the manipulated image data to a morphological operation, and extracting features relating to the trabecular structure from the estimated projected trabecular pattern,

    (d)   obtaining, on the basis of a frequency analysis of the image data, features relating to the periodicity of the trabecular structure of the part of the bone,

- and an estimation procedure in which the bone quality of the vertebrate is estimated on the basis of the derived features and optionally other features related to the

bone or the vertebrate and a predetermined relationship between the values of such features and reference bone quality parameters.

As indicated above, in the present context "bone quality" is
5   not equalled to "bone quantity", such as Bone Mineral Density, as even a small loss of bone quantity may lead to a large loss of bone quality if the bone loss has taken place at critical positions in the trabecular structure. Thus, in the present context "bone quality" is a measure closely
10   related to the risk of fracture of the bone, as it has been demonstrated in stress/strain evaluations of bone biopsies in which the microscopic structure is also evaluated (See, e.g., Lis Mosekilde relating to this issue).

Even though the bones and, thus, the trabecular structures
15   are inherently three-dimensional, a projection of this structure into two dimensions, such as a radiographic image, yielding a so-called projected trabecular pattern, conveys sufficient information about the trabecular structure and, thus, the bone quality to give a satisfactory estimate of the
20   bone quality.

Information relating to the trabecular structure may be local variations in, e.g., grey level information or any other information from which features relating to the trabecular structure may be derived.

25   Low frequency intensity variations in the image data will naturally depend on how the image data are obtained. If the image data are obtained on the basis of radiographic images, the low frequency intensity variations may be due to, e.g., scattering of the electromagnetic radiation, anatomic struc-
30   tures surrounding the illuminated part of the trabeculae such as cortical bone, fat tissue and muscles of varying thickness as well as, e.g., inhomogeneous X-ray illumination of the part of the bone.

According to the first aspect of the present invention, local image intensity information and variation in the local intensity are utilized to extract information relating to the trabecular structure of the part of the bone. In, e.g.,
5   digitized radiographic images, local image intensity information may be the individual pixel values, whereas variation in the local intensity is related to the textural information contained in, e.g., inhomogeneities in the image data.

The extracted features resulting from the image manipulation
10 and feature extraction procedure quantify properties of the trabecular structure and, thus, of the bone quality. The extracted features are subsequently introduced into an estimation procedure in which a predetermined relationship between features and bone quality enables the estimation
15 procedure to estimate the bone quality of the vertebrate.

In the present context, to "emphasize" information, such as magnitude information, means to give prominence to prevailing frequency information. This may be performed by either enhancing the prominent information or by reducing the less domi-
20 nant information - optionally both.

According to the first aspect of the invention, an estimate of the bone quality is obtained in an estimation procedure on the basis of a predetermined relationship between features obtained and reference bone quality parameters. This prede-
25 termined relationship is typically established through statistical modelling, where explanatory variables (image features and optionally other explanatory features relating to the bone quality) are used to model corresponding reference bone quality data (response variable).

30 As described above, even though bone quality is not equal to bone quantity in the present context, the reference bone quality parameters are preferably parameters related to the strength of the bone rather than, e.g., BMD or BMC which, as explained above, relate to the density of the bone rather

than the strength thereof. However, to provide even higher
diagnostic sensitivity, combination of the present invention
with a measurement of BMC/BMD is contemplated to be useful.
BMC/BMD measurements can be obtained either by the above-
5 mentioned two-wavelength-technique or they may, if the image
data are obtained on the basis of an X-ray image, be avail-
able from the same image data, where, e.g., a standard alu-
minum wedge has been illuminated together with the bone in
question.

10 At present, the most common way of obtaining non-invasive
information about the bone quantity and bone quality is based
on X-ray illumination. X-ray images may easily be used to
generate the image data for use in the present invention. As
it is preferred to perform the statistical analysis on a
15 computer, the analogue X-ray image may be digitized and
introduced into a computer by scanning the X-ray image.

Naturally, the resolution of the X-ray film used to obtain
the X-ray image will have an effect on the quality of the
image data. Thus, it is presently preferred that the resol-
20 ution of the X-ray film is at least 4 pairs of lines per
centimetre, such as at least 5 pairs of lines per centimetre.
Even though this may be sufficient for obtaining a satisfac-
tory estimation of the bone quality, it is preferred that the
resolution of the X-ray film is at least 10 pairs of lines
25 per centimetre, such as at least 25 pairs of lines per centi-
metre, preferably at least 50 pairs of lines per centimetre.
It is possible to obtain resolutions of the X-ray film up to
at least 100 pairs of lines per centimetre, such as at least
250 pairs of lines per centimetre and probably as high as 500
30 pairs of lines per centimetre, such as at least 600 pairs of
lines per centimetre. Naturally, a resolution of this
preferred size will ensure that a large amount of information
is present in the X-ray image.

Naturally, it is preferred that the scanning of X-ray images
35 is performed with a sufficiently large resolution in order to

ensure that a minimum relevant information of the X-ray image
is lost in the transfer to the image data. Thus, it is pre-
ferred that the scanning has been performed at a resolution
of at least 10 lines per cm, such as at least 25 lines per
5   cm, preferably at least 100 lines per cm, such as at least
200 lines per cm, such as at least 250 lines per cm.

Furthermore, it is preferred that the resolution of the
scanner is better than 4 true bits per pixel, such as better
than 6 true bits per pixel. preferably better than 8 bits per
10   pixel.

Naturally, in order to have the scanner actually scan the
image, it should be able to transilluminate the radiographs.

The ESKOSCAN 2450 from Eskofot A/S has been found to fulfil
the above criterias and to be highly suited for use in the
15   method of the invention.

It is presently preferred that the background correction
procedure comprises at least reducing or optionally removing
low frequency information having a frequency significantly
lower than the spacing of the projected trabeculae. As
20   described above, this low frequent spectral content of the
image data is typically caused by cortical bone, fat tissue
and muscles of varying thickness as well as, e.g.,
inhomogeneous X-ray illumination of the part of the bone.
Naturally, this type of undesirable effect is unavoidable
25   when obtaining non-invasive image data on the basis of X-ray
radiographs. However, other non-invasive image acquisition
techniques, such as, e.g., MR and CT imaging may generate
image data not automatically or not to the same degree "suf-
fering from" this type of undesired effect.

30   Even though it is difficult to exactly quantify the limit
between undesired low frequency information and the desired
higher frequency relevant information independently of the
image resolution, it is presently preferred that information

having frequencies half or less than the spacing of the
projected trabeculae is at least reduced or optionally
removed. More preferably, information having frequencies
being a quarter or less, such as a tenth or less than the
5   spacing of the projected trabeculae is at least reduced or
optionally removed.

One preferred way of reducing or preferably removing the low
frequency information is using a background correction pro-
cedure comprising generating secondary image data as a result
10 of performing a median filtering with a predetermined kernel
size and subtracting this result from the original image
data. One of the advantages of using a median filter is that
this operation is edge preserving.

Another way of reducing or preferably removing the low fre-
15 quency information is using a background correction procedure
comprising generating secondary image data as a result of
performing a mean filtering with a predetermined kernel size
and subtracting this result from the original image data. A
mean filtering is typically much faster than the median
20 filtering. However, the mean filtering is not edge preser-
ving. Edges generated in this part of the process may have an
adverse effect and generate false or erroneous information
later in the process, leading to wrong estimates of the bone
quality.

25 It is typically preferred that the kernel size is at the most
1/2 of the image data, such as at the most 1/4 of the image
data, preferably at the most 1/10 of the image data, more
preferably at the most 1/20 of the image data.

A third way of reducing or preferably removing the low fre-
30 quency information is using a background correction procedure
comprising globally fitting a two-dimensional polynomial to
the image data and generating background corrected image data
on the basis of the residuals of the fitting procedure. Apart
from potential difficulties in determining the optimal order

of the polynomial, which the person skilled in the art will
know, this method potentially offers an extremely fast back-
ground correction of image data.

It is contemplated that a suitable order of the polynomial
5 may be at the most 15, such as at the most 10, more preferab-
ly at the most 5.

Having performed a background correction of the image data,
an image manipulation and feature extraction procedure is
performed in order to obtain features quantifying textural
10 properties of the trabecular structure.

An important textural property relating to the bone quality
is the degree of anisotropy of the projected trabecular
pattern. This property may be described in an intuitively
appealing way using the power spectrum of the image data. The
15 power spectrum may be obtained using direct methods, auto-
covariance methods or parametric methods.

Classical spectral estimation, however, which comprises
direct methods and auto-covariance methods, typically gives
relatively non-consistent spectral estimates with a poor
20 resolution. Alternatively, smoothing methods may be employed.
This, however, brings about the well-known
variance/resolution trade-off.

Therefore, parametric spectral estimation is used according
to the invention as this estimator is a consistent spectral
25 estimator with superior resolution properties.

One way of obtaining the parametric estimate of the power
spectrum is subjecting the image data, optionally weighted
with a window, to a Fast Fourier Transformation. This is a
so-called direct method of which there are several variants,
30 where the most popular probably is the so-called Welch
method.

Another way of obtaining the parametric estimate of the power
spectrum is subjecting an estimate of the auto-covariance
function of the image data, optionally weighted with a
window, to a Fast Fourier Transformation.

5   As mentioned above, the parametric methods potentially offer
a higher resolution than the classical methods. The basic
principle of parametric methods is to identify an appropriate
model of the image data, which is assumed to be a homogeneous
texture, and subsequently estimate the parameters of the
10 model. Having estimated these parameters, the parametric
estimate of the power spectrum of the fitted model may be
obtained. In one dimension, this type of spectral estimate
has proven itself superior to the classical spectral
estimates.

15 The methods, on the basis of which the parametric estimate is
obtained are at present preferably chosen from the group
consisting of: causal Simultaneous Auto-Regressive Moving
Average (SARMA) models, non-causal SARMA models, Gaussian
Markov Random Field models and Maximum Entropy Spectral
20 Estimates.

When considering spatial data, such as image data, causality
is not natural. Abandoning causality, however, leads to
serious problems in the estimation of the parameters as the
Least Squares estimator is no longer consistent. Therefore,
25 it is often preferred to superimpose an artificial
directionality on the image data. Thus, having a causal
model, the Least Square estimation principle may be applied.

However, a disadvantage of superimposing an artificial
directionality on the image data is the so-called "direc-
30 tional bias" which may be quite conspicuous in, e.g., the
estimate of the parametric estimate of the power spectrum.
Consequently, the use of causal models in the present context
is not an obvious choice. This problem is partly solved using
the "parallel-resistor" averaged spectral estimator

introduced by Chan in ("Two-dimensional Spectral estimation from Auto-regressive Models with varying Areas of Support" from 1981).

Hitherto, when considering non-causal models, one has been
5   forced to consider the Maximum Likelihood Estimator, which gives a number of practical problems for the following reasons:

-   The Likelihood function includes the determinant of the Jacobian matrix which is of the size $M^2 \times M^2$ (where M in
10   the 2-D situation is the side length of the image). This determinant is a complicated non-linear function of the model parameters.
-   Even if assumptions are made about the image (e.g. torus) that offers an analytical expression for the above-men-
15   tioned determinant, the computational load will still be very large.
-   Close to non-stationarity, the Likelihood function is extremely rippled. This will often cause the non-linear optimization routine to find a sub-optimal solution to
20 .   the estimation problem. It is not feasible/possible to test for this in two dimensions or more, due to the computational effort required.

For the above-mentioned reasons, the Maximum Likelihood estimation is not a practical way of obtaining estimates of
25 the model. Other estimation principles may, of course, be more practical alternatives.

At present, it is preferred that the method on the basis of which the parametric spectrum is obtained, is a non-causal SARMA model using the so-called MORSE estimator. This estima-
30 tor will be described further below.

Having obtained the parametric estimate of the power spectrum of the image data, one or more features are extracted which quantify properties of the bone quality.

The distribution of the energy in the parametric estimate of
the power spectrum relates directly to the anisotropy of the
image data. Thus, several types of features may be proposed
which quantify this anisotropy.

5   At present, it is preferred to obtain at least one feature
    related to parameters of a contour encompassing at least a
    predetermined percentage of the energy of the parametric
    estimate of the power spectrum.

    This the contour may, e.g., is determined by

10 (a)   defining a contour, in terms of one axis in each
            dimension, around the centre of the parametric
            estimate of the power spectrum, all points on the
            contour having substantially the same distance to the
            centre of the parametric estimate of the power
15   spectrum, and the contour encompassing less than the
            predetermined percentage of the energy of the
            parametric estimate of the power spectrum,
    (b)   for each dimension of the data calculating the per-
            centage of the energy of the parametric estimate of
20   the power spectrum encompassed by a dilated contour
            in which the axis in the dimension in question is
            increased by a predetermined distance,
    (c)   increasing the axis of the contour, in the dimension
            in which the increase in energy encompassed by the
25   dilated contour is the largest, by the predetermined
            distance and
    (d)   repeating steps (b) and (c) until the percentage
            encompassed by the contour exceeds or equals the
            predetermined percentage.

30 The distribution of energy in the parametric estimate of the
    power spectrum is typically oblong. Tests have shown that the
    distribution of the energy in the parametric estimate of the
    power spectra of osteoporotic patients differ significantly
    from those of non-osteoporotic persons. This difference may,

e.g., be seen in a difference in the area covered by or the
elongatedness of the above-mentioned contour.

One way of obtaining suitable features from the contour is to
define the shape of the contour and subsequently derive
5 features from parameters of the contour.

A suitable way of defining the contour is to define the axes
of the contour so that these are orthogonal and directed
along principal directions of the parametric estimate of the
power spectrum.

10 A natural shape of this contour may be an ellipsoidal contour
and one or more features may be derived from the semi-axes
thereof. However, a rectangular contour may also be used.

The above-mentioned method of defining the contour is prefer-
ably performed so as to obtain the smallest possible contour
15 of the desired shape. This will ensure that the contour is
uniquely defined and that the features derived from parame-
ters of the contour relate as well as possible to the anisot-
ropy of the image data.

An alternative way of extracting information in the frequency
20 domain is to derive information from e.g. the height, width
or total area under peaks of a smoothed periodogram. From
this information, features relating to periodicity of the
trabeculae may be derived. In this manner, information
relating to a periodicity of the trabeculae is obtained by
25 performing a frequency analysis of the image data.

Several other ways of extracting features from the parametric
estimate of the power spectrum may be used, such as fitting a
Gaussian to the normalized parametric estimate of the power
spectrum and deriving features from this Gaussian. Other
30 methods are using rings and wedges as described by Weszka et
al. (1976).

An image manipulation and feature extraction method alterna-
tive to or supplementing the above use of the parametric
estimate of the power spectrum is to estimate the projected
trabecular pattern of the image data by using a Fourier
5   method to emphasize the information in the image data
relating to the trabecular structure and subjecting the
manipulated image data to a morphological operation, and
extracting features relating to the trabecular structure from
the estimated projected trabecular pattern.

10   The emphasizing procedure is essential in order to bring out
the projected trabecular pattern in a robust manner. To this
end, Fourier methods have proven suitable, and it is pre-
ferred that the Fourier method comprises
     -    subjecting the image data to Fourier transformation,
15   -   performing a subsequent mathematical transformation of
          the Fourier transformed data,
     -    converting the transformed data back into the spatial
          domain.

Naturally, the subsequent mathematical transformation may be
20   linear or non-linear.

Even though it is preferred that the subsequent mathematical
transformation is performed by raising the magnitude of the
Fourier transformed data to a power larger than 1, such as a
power in the range of 1.1-10, preferably 1.5-4, such as about
25   2.0, also other transformations, such as other types of
filtering, may be performed.

In order to further emphasize the information relating to the
trabecular structure, a third mathematical transformation may
be performed in order to preserve only part of the magnitude
30   information of the transformed data. This may, e.g., be
removal of at least part of the information in the magnitude
of the spectrum.

Having emphasized the information in the image data relating
to the trabecular structure, the resulting image data is
preferably subjected to grey-scale morphological operations
in order to prepare the data for feature extraction.

5   At present, the purpose of the grey-scale morphological
operations is to extract a binary representation of the
projected trabecular pattern (PTP). The foreground colour
represents the trabeculae, whereas the background colour
represents the cavities.

10   The above PTP is preferably obtained using the so-called
morphological top-hat operation followed by a thresholding.
The result of these operations is preferably further
"cleaned" by removing small isolated clusters of pixels.

On the basis of the PTP obtained, a number of different
15   features may be obtained. In the following, the generation of
just a few of the vast number of possible features is
described.

One method of generating features from the PTP is performing
an operation (the so-called "distance transform") comprising
20   determining, for each background pixel, the distance accord-
ing to a given metric from the background pixel to the
nearest foreground pixel. The features extracted from this
operation are indeed intuitively appealing as they relate
directly to the inter-trabecular distance.

25   The above metric is presently the Euclidian distance. How-
ever, other metrics may eventually prove more suitable in the
present context.

Features based on the distance transform may, e.g., be
derived from a mean value and/or standard deviation and/or
30   the coefficient of variation and/or skewness and/or kurtosis
of the determined distances.

Another method of generating features from the PTP is per-
forming an operation (hereinafter referred to as "star area
transform") comprising determining a measure for each back-
ground pixel based upon determining the distance from the
5   background pixel to the nearest foreground pixel in a number
of given directions in the image data.

Again, features derivable from the star area transform may,
e.g., relate to a mean value and/or standard deviation and/or
the coefficient of variation and/or skewness and/or kurtosis,
10   optionally the maximum distance, of the determined measures.

In addition to the above-mentioned features derivable from
the image data, it may be preferred to input additional data
into the estimation procedure. It is evident that a large
number of features which relate to the illuminated bone, but
15   which are not derivable from the image data, may enhance the
precision of the estimation of the bone quality.

As the present method may be used to estimate the bone qual-
ity of any bone from any vertebrate, additional information
as to the age and/or sex, and/or species, and/or race and/or
20   the specific bone considered in the vertebrate, and/or a
estimated Bone Mineral Density, and/or a estimated Bone
Mineral Content, may be included in the estimation procedure.

Even though the BMD may be introduced in the estimation
procedure, this measure may also optionally be determined
25   from the image data. BMD may be estimated by including data
from a reference object in the exposure of the bone to the
electromagnetic radiation and on the basis of the absorption
of the electromagnetic radiation of the bone and of the
reference object.

30   The purpose of the estimation procedure is to estimate given
bio-mechanical properties of the bone on the basis of the
introduced features extracted from the image data and other
explanatory variables.

One way of obtaining an estimation procedure of the above type is to have the estimation procedure based on a statistical model, taking into account the correlation structure in the data set, so as to assign appropriate weights to the

5   significant features in accordance with the predetermined relationship.

The above-mentioned model may be determined in a number of ways. However, establishing a model of this type requires obtaining corresponding values of all relevant features and a

10   response variable relating to the bio-mechanical property which is to be estimated by the estimation procedure. The bio-mechanical property in question may be an absolute or a relative measure of the bone quality.

Examples of interesting bio-mechanical properties of bone are

15   the mechanical bone strength, and/or a Bone Mineral Density measurement, and/or a Bone Mineral Content measurement, and/or a score value by a skilled radiologist. Naturally, the method of the present invention will output a value corresponding to the calibration of the method: if the method is

20   calibrated towards a strength parameter, the output of the method will relate to the strength of the bone in question.

An important purpose of the present invention is to provide a method for evaluating bone strength and fracture risk of significant clinical value, thus to provide a higher estima-

25   tion of fracture risk than the best technique available today, the Double X-ray Absorptiometry Bone Mineral Content measurements (DXA-BMC measurements).

As the calibration of the estimation procedure will determine the estimated parameter of the bone, this parameter should be

30   chosen in a manner so that it correlates to the bone quality. The assessment of the extent to which the embodiments of the present invention are able to estimate bone quality may be performed by:

1. Cohort-studies, in which occurrence of new fractures are recorded and related to the initial estimation,

2. cross-sectional studies, in which fracture cases and age-and-sex-matched controls are compared to estimations

5   obtained by the method according to the invention and option-
ally further to DXA-BMC measurements, or

3. by using bio-mechanical testing of bone specimens, pre-
ceded by estimating the bone quality according to the inven-
tion and optionally additionally DXA-BMC-measurements of the

10   bone in question.

Using either distal radius, lumbar spine, femoral neck, or
any bone in which two-dimensional image data comprising
information relating to the trabecular structure the bone can
be obtained, coherent values for determined bone strength,

15   DXA-BMC and the estimate according to the present invention
may be performed on the basis of human post-mortem bone
samples or samples from other vertebrates.

The calibration of the method of the present invention may
also be calibrated along the above-illustrated methods as

20   these methods generate bone quality information and estima-
tion on the basis of corresponding image data.

Bone strength may, e.g., be evaluated by directly measuring
the plasticity and maximum load of a bone in a stress-strain
diagram (See, e.g., Lis Mosekilde). These parameters are

25   preferably obtained in both the direction of the vertical
trabeculae and in the orthogonal direction in order to have
the most complete estimate of the bone quality.

In the method of the invention, substantially all types of
models may be used in the estimation procedure. At present, a

30   preferred model is selected from the group consisting of: a
General Linear Model, a Generalized Linear Model, an Artifi-

cial Neural Network, a Causal Probabilistic Net or Classifi-
cation And Regression Trees.

As described above, the present method may be used to esti-
mate the bone quality of bone in any vertebrate. Thus, the
5   vertebrate may be a human, a horse, a great ape, a large ape,
an anthropoid ape, a pig, a cow, etc, and the actual bone may
naturally be virtually any bone in the vertebrate, such as
radius, femur, corpus vertebrae, calcaneus, talus, os carpi,
metatarsi, metacarpi, falanges, tibia, fibula, patella, ulna,
10   humerus, mandible, clavicula, scapula, os coxae, os
naviculare, os cuboideum, os cuneiform I, os cuneiform II or
os cuneiform III.

A second aspect of the present invention relates to a method
for estimating the bone quality of a vertebrate, on the basis
15   of two-dimensional image data comprising information relating
to the trabecular structure of at least a part of a bone of
the vertebrate, the image data being data obtained by expos-
ing at least the part of the bone to electromagnetic radi-
ation, the method comprising subjecting the image data to a
20   statistical analysis comprising

-    a background correction procedure in which low frequent
     intensity variations not related to the trabecular struc-
     ture of the bone is reduced relative to image data
     related to the trabecular structure of the part of the
25   bone,
-    an image manipulation and feature extraction procedure
     comprising subjecting the image data to at least one of
     the following procedures:
     (a)   obtaining an estimate of the parametric estimate
30   of the power spectrum of the image data and
               extracting features relating to the energy
               distribution of the parametric estimate,
     (b)   obtaining, on the basis of image data on which a
               Fourier method has been used to emphasize the
35   information in the image data relating to the

trabecular structure, an estimate of a grey-level
co-occurrence matrix and extracting at least one
feature on the basis of the estimated co-occur-
rence matrix,

5   (c)   obtaining an estimate of the projected trabecular
pattern of the image data by using a Fourier
method to emphasize the information in the image
data relating to the trabecular structure and
subjecting the manipulated image data to a mor-
10   phological operation, and extracting features
relating to the trabecular structure from the
estimated projected trabecular pattern,

(d)   obtaining, on the basis of a frequency analysis
of the image data, features relating to the
15   periodicity of the trabecular structure of the
part of the bone,

-     and an estimation procedure in which the bone quality of
the vertebrate is estimated with a Multiple Correlation
Coefficient better than 0.5 on the basis of the derived
20   features and optionally other features related to the
bone or the vertebrate and a predetermined relationship
between the features and reference bone quality parame-
ters.

In fact, the bone quality of the vertebrate is preferably
25   estimated with a Multiple Correlation Coefficient better than
0.55, such as better than 0.6. Naturally, the higher the
Multiple Correlation Coefficient the higher the correlation
between the actual bone quality and the estimated bone qual-
ity. Thus, a Multiple Correlation Coefficient better than
30   0.65, such as better than 0.7, or better than 0.8, such as
better than 0.85 is preferred in order to have as high a
correlation to the actual value as possible.

In a third aspect, the present invention relates to a method
for estimating Non-Causal Simultaneous Auto-Regressive Moving
35   Average models in two or more dimensions, the method compris-
ing optimizing a given direct measure of the flatness of the

residual spectrum of the model. In the present context
"optimizing a given direct measure of the flatness" means
that the flatness is maximized.

Non-linear optimization procedures are typically used to
5   maximize measures of the above type. A suitable non-linear
procedure may comprise the following steps
    (a)   generating a set of initial parameters for the model,
    (b)   generating the residual spectrum of the model on the
             basis of the parameters,
10   (c)   obtaining the measure of the flatness of the residual
             spectrum,
    (d)   obtaining a new iterate of the parameters on the
             basis of the flatness measure and a search direction
             in parameter space,
15   (e)   repeating steps (b)-(d) until given stop criterion is
             reached.

A number of measures of the flatness of the residual
parametric estimate of the power spectrum may be chosen. A
well known measure of flatness of probability distributions
20   is the so-called entropy. Therefore, in the present context,
the entropy is measured on the normalized residual parametric
estimate of the power spectrum, disregarding the DC value.

Preferred embodiments of aspects of the invention will now be
described with reference to the drawings wherein

25   Fig. 1 shows a typical radiographic image of a wrist,
obtained by an ESKOFOT scanner (See Example 1),

Fig. 2 shows an extracted sub-image of the image of Fig. 1,

Fig. 3 shows the image of Fig. 2 after a median filtering
with a 25×25 kernel size,

30   Fig. 4 shows the final background corrected image,

Fig. 5 shows the power spectrum of the background corrected image of Fig. 4,

Fig. 6 shows the restored result of the image of Fig. 4 after having been subjected to an emphasizing procedure,

5   Fig. 7 shows the result of a morphological top-hat operation on the restored image of Fig. 6,

Fig. 8 shows the image of Fig. 7, wherein small isolated groups of pixels (noise) have been removed (this image is referred to as the projected trabecular pattern (PTP)),

10   Fig. 9 shows the result of a distance transform calculated for the PTP of Fig. 8,

Fig. 10 illustrates the star area transform for a single pixel.

Fig. 11 shows the result of the star area transform of all
15   background pixels in the PTP of Fig. 8,

Fig. 12 shows the result of the maximum distance transform of the PTP of Fig. 8,

Fig. 13 shows the smallest possible ellipse containing 70% of the spectral energy for a 'normal' patient,

20   Fig. 14 shows the smallest possible ellipse containing 70% of the spectral energy for an osteoporotic patient,

Fig. 15 illustrates the systematic bias of the LS estimates for simulated isotropic textures (the vertical lines along the curve outline the empirical confidence intervals for the
25   mean of the estimated parameters(,

Fig. 16 illustrates the systematic bias of the approximative ML estimates (close to non-stationarity) for simulated

isotropic textures (the vertical lines along the curve out-
line the empirical confidence intervals for the mean of the
estimated parameters),

Fig. 17 illustrates a part of the likelihood function for a
5   first-order bilateral SAR model (given a realization of the
process with the parameters $\alpha=\beta=-0.22735$. The likelihood is
plotted in the interval $(\alpha,\beta)\in[-0.275,-0.20]\times[-0.275,-0.20]$),

Fig. 18 illustrates that good estimates may be obtained using
the torus-ML estimator with the approximate ML estimates as
10 initial values combined with a stationarity check (if a
non-stationary solution model is found, the optimizer is
restarted with new initial values; the vertical lines along
the curve outline the empirical confidence interval for the
mean of the estimated parameters),

15 Fig. 19 illustrates that good estimates may be obtained using
the MORSE estimator (the vertical lines along the curve is
the empirical 95% confidence intervals for the mean of the
estimated parameters),

Fig. 20 shows the objective functional of the MORSE estimator
20 close to non-stationarity (as opposed to, e.g., the ML-estim-
ator, this objective functional is not rippled, which makes
it much easier to perform the non-linear optimization),

Fig. 21 illustrates the periodogram estimator of the power
spectrum for a normal individual (left) and for an
25 osteoporotic individual (right). The spectrum is shown in
inverse so that the high intensity values are darker than the
lower intensity values,

Fig. 22 illustrates the parametric NSHP estimate of the power
spectrum for a normal individual (left) and for an
30 osteoporotic individual (right). The spectrum is shown in
inverse so that the high intensity values are darker than the
lower intensity values,

Fig. 23 illustrates the parametric WQP estimate of the power spectrum for a normal individual (left) and for an osteoporotic individual (right). The spectrum is shown in inverse so that the high intensity values are darker than the
5 lower intensity values,

Fig. 24 summarizes an experiment performed in order to describe the applicability of the MORSE estimator,

Fig. 25 illustrates histograms based on parameters estimated for each of 1000 synthesized 128x128 textures,

10 Fig. 26 illustrates optimal strengths plotted against the predicted strength, where age is not included in the model,

Fig. 27 illustrates optimal strengths plotted against the predicted strength, where age is included in the model, and

Fig. 28 illustrates the correlation of the logarithmic
15 optimal fracture load and a single feature suitably chosen.

EXAMPLE 1: Textural analysis of bone structure

In the following Example, a preferred embodiment of the method of the invention will be described wherein X-ray images of the distal radius and a vertebral body from the
20 lumbar spine (L3) are restored using image processing. The restored images are used as a basis for extracting textural features that are shown to correlate well with the structure, the density and the fracture load of the trabecular bone. Several ways of extracting promising textural features are
25 described. A model based on textural features (and possibly age and sex) is described and shown to discriminate well between osteoporotic and non-osteoporotic cases.

Obtaining suitable image data

The X-ray images used in this Example were obtained using a
standard X-ray instrument having a focus area of 0.6 mm^2, a
tube voltage of 45 kV, a focus-to-foil distance of 100 cm, a
5 single, fine X-ray foil (it should be noted that no foil is
required), using a double emulsion film (it should be noted
that a single emulsion film is equally applicable) and adjus-
ting the MAS product to obtain a suitably exposed film.

The X-ray pictures were scanned into a computer using a
10 ESKOFOT ESKOSCAN 2450 scanner capable of scanning up to 5000
lines/cm. However, at present 600 lines/cm was used. This
scanner was found highly suited for the present use. A typi-
cal image is shown in Fig. 1.

The demands to a scanner suitable for this use are that it
15 should naturally be able to transilluminate the X-ray film,
it should preferably have a resolution better than the grains
in the film/foil combination (so as to loose no information
in the scanning procedure) and it should preferably generate
grey-values of at least 8 true bits, in order to obtain a
20 suitable dynamic range of the image data.

Spatial Texture Models

Preprocessing

In this study, only the textural information is taken into
account. Therefore a sub-image is extracted in a region of
25 the bone containing only trabecular bone, as e.g. shown in
Fig. 2. Low frequent intensity variations due to, e.g.,
scattering of the radiation, anatomic structures as cortical
bone, muscles, fat tissue of varying thickness etc., are
removed by subtracting a median filtered version of the image
30 (shown in Fig. 3) from the image itself (a technique known as
"unsharp filtering"). In this case a 31x31 median filter is
used. The background-corrected image is shown in Fig. 4. This

image is very noisy and should be further processed prior to further transformations and subsequent feature extraction.

The noise in the image is clearly very high-frequent, whereas the information which is preferably considered (the trabecular structure) is of a more low-frequent nature.

The power spectrum of the extracted, background corrected sub-image is shown in Fig. 5. In the following, an emphasizing procedure will be described, which may not be generally applicable for removal of high-frequent noise, but tends to emphasize the dominating (in this case low-frequent) features in the images, while suppressing less dominating (in this case high frequent noise) features. This property makes it attractive for this specific purpose.

Algorithm 1   The following steps outline the restoration algorithm that removes high-frequent noise and emphasize the relevant structures in the image.

1. Perform a 2-D FFT and obtain the phase, $X_P(f_r, f_c)$, and the magnitude, $X_M(f_r, f_c)$.

2. The magnitude is raised to the power p:

$$S(f_r, f_c) = |X_M(f_r, f_c)|^p \tag{1}$$

3. The histogram of $S(f_r, f_c)$ is stretched to match a Gaussian: $S_G(f_r, f_c)$

4. A context image, $C(f_r, f_c)$, is formed by thresholding $S_G(f_r, f_c)$ preserving T% of the pixels. Objects less than n pixels are removed from the thresholded image. (note that more than T% of the energy is preserved).

5. A 'new' magnitude image, $X_N(f_r, f_c)$, is formed using the context image and the power spectrum (not the magnitude):

$$X_N(f_r, f_c) = \begin{cases} S(f_r, f_c) & \text{if } C(f_r, f_c) = 1 \\ 0.0 & \text{otherwise} \end{cases} \qquad (2)$$

6. The new magnitude image $X_N(f_r, f_c)$ is combined with the
phase image $X_P(f_r, f_c)$, and the restored image, $\chi_R(r,c)$, is
obtained as the real part of the inverse Fourier transform.
It is preferred to use thresholding in the range T=1-6 and
5   p=1-2.

Note that the magnitude, raised to the power p, is used to
form the new magnitude image. This may not be obvious, but it
has been experienced that this in general provides very
useful results. The reason for this is, that when the
10   magnitude is raised to a given power larger than one, the
parts of the spectrum that contain most of the energy tend to
be emphasized whereas spectral components with less energy
tend to be weakened further. The result of the emphasizing
procedure using T=2 and p=2 is shown in Fig. 6.
15

Extraction of the PTP

In the following, various image transformations and textural
features, extracted from transformed images, will be dis-
cussed. Several features are based upon an image subsequently
20   referred to as the projected trabecular pattern (PTP) which
is obtained as outlined below:

Algorithm 2   The steps outlined below describe the desired
transformations of the restored image in order to measure a
relevant set of features on the resulting PTP.

25   1. Perform the grey-scale morphological top-hat opera-
            tion on the restored image. The top-hat operation is
            the original image minus an opened version of the
            image. This image is subsequently thresholded. The
            result of these operations is shown in Fig. 7.

2. This image clearly contains a lot of noise-pixels.
    Small isolated objects (in the present Example all
    objects less than 10 pixels) are removed. The result-
    ing PTP is shown in Fig. 8.

5   *Extraction of Statistical Features*

    Naturally, it is preferred to extract features that, in some
    sense, quantify the properties (such as structure and
    density) of the trabecular structure. Not surprisingly, the
    meshes of the PTP-net are much larger, and often broken, for
10 osteopenic individuals than for non-osteoporotic individuals.
    This difference may be quantified in several ways. Such
    properties are, e.g., reflected in the average distance from
    each background pixel to the nearest foreground pixel
    (bone-pixel) in the projected trabecular pattern.

15 The size of the dark meshes in the pattern is a relevant
    parameter that is conveniently quantified by calculating the
    so-called distance transform for the projected trabecular
    pattern. The result of the distance transform on the PTP is
    shown in Fig. 9 and is denoted $\chi_D(r,c)$.

20 In addition, for each background pixel in the projected
    trabecular pattern, a line is drawn from the pixel, in a
    given direction, until a foreground pixel ('bone-pixel') is
    found. The distance between these pixels is measured. This is
    done for a fixed number of directions as illustrated in Fig.
25 10. After this, the *average* distance which is referred to as
    the *star area*, denoted $\chi_A(r,c)$, or the *maximum star length*
    which is denoted $\chi_X(r,c)$ may be calculated. These images are
    shown in Fig. 11 and Fig. 12 respectively.

    A number of statistical moments may be calculated from the
30 resulting images from the measured average, standard
    deviation, coefficient of variation and skewness for all
    background pixels:

$$\hat{\mu}. = \frac{1}{N} \sum_{r,c} \chi.(r,c) \tag{3}$$

$$\hat{\partial}. = \frac{1}{N} \sum_{r,c} (\chi.(r,c) - \hat{\mu}.)^2 \tag{4}$$

$$c\hat{\upsilon}. = \frac{\hat{\partial}.}{\hat{\mu}.} \tag{5}$$

$$\hat{\varphi}. = \frac{\sum_{r,c} (\chi.(r,c) - \hat{\mu}.)^3}{\hat{\partial}.^3} \tag{6}$$

where the subscript denotes different transforms considered:

- D: Distance transform
- M: Mean value of star length
- S: Standard deviation of star length
- X: Maximum star length
- A: Star area

We briefly outline the interpretation of the considered parameters:

The $\hat{\mu}.$ and $\hat{\sigma}.$ features are either related to the general mesh size (for D, M, A and X) or the degradation of the mesh (S). For example, larger mesh sizes are reflected in a larger value of $\hat{\mu}.$. Thus, for increasing values of $\hat{\mu}.$ and $\hat{\sigma}.$, the texture index should decrease.

The cv. feature is somewhat different. It measures the width of the empirical distribution in the transformed images. If all the distances are large, cv. would be small. The same thing would be the case, if all the distances were small. Typically, however, we find that the empirical distribution

is wide, only if the PTP mesh is broken. Thus, for increasing values of $\hat{cv}.$, the texture index should typically decrease.

The $\hat{\gamma}.$ feature is also related to the mesh size. If the histogram of distances is heavier in the right side, $\hat{\gamma}.<0$. If the empirical distribution is symmetrical, $\hat{\gamma}=0$. For large meshes in the PTP, the distribution of distances would typically be skewed for large values. Thus, for increasing values of $\hat{\gamma}.$, the texture index should decrease.

Textural Features Extracted in the Spatial Frequency Domain

One would intuitively think that features measured in the frequency domain should carry relevant information about the trabecular structure. The trabecular structure for strongly osteoporotic patients is clearly more low frequent than that for 'normal' patients. In the present section, the considered Fourier features are not measured on the projected trabecular pattern. Instead, the features are measured on the spectrum of the background corrected image.

Preprocessing

Before estimating the spectrum, non-stationaries of the extracted image are removed by subtracting a 31x31 median filtered version of the image from itself as described above.

Spectral Estimation

As the main interest is directed toward the relatively low-frequent properties of the power spectrum, a weighed estimate of the dispersion may be used, where $p^*(u,v)$ is the normalized power spectrum taking a weight function into account:

34

$$P^{\bullet}(u, v) = \frac{P(u, v) \cdot w(u, v)}{\sum_{(u,v) \neq (0,0)} P(u, v) \cdot w(u, v)} \tag{7}$$

and

$$w(u, v) = \frac{1}{u^2 + v^2} \tag{8}$$

Given a positive definite symmetrical matrix

$$\Sigma = \begin{pmatrix} \sigma_u^2 & \sigma_{uv} \\ \sigma_{uv} & \sigma_v^2 \end{pmatrix} \tag{9}$$

the eigenvalues are:

$$\lambda_1 = \frac{\left(\sigma_u^2 + \sigma_v^2 + \sqrt{(\sigma_u^2 - \sigma_v^2)^2 + 4\sigma_{uv}^2}\right)}{2} \tag{10}$$

$$\lambda_2 = \frac{\left(\sigma_u^2 + \sigma_v^2 - \sqrt{(\sigma_u^2 - \sigma_v^2)^2 + 4\sigma_{uv}^2}\right)}{2} \tag{11}$$

5 and the corresponding (normalized) eigenvectors

$$\underline{P_i}^T = \left(\frac{\sigma_{uv}}{\sqrt{\sigma_{uv}^2 + (\lambda_i - \sigma_u^2)^2}} ; \frac{\lambda_i - \sigma_u^2}{\sqrt{\sigma_{uv}^2 + (\lambda_i - \sigma_u^2)^2}} \right) \tag{12}$$

An alternative estimate of the power spectrum may be obtained from the following process:

The probably best known estimator of the power spectrum is the periodogram estimator:

$$I(u, v) = \frac{1}{M^2} \left| \sum_{m=0}^{M-1} \sum_{n=0}^{M-1} y(m, n) \exp\left(-i2\pi \left(\frac{um}{M} + \frac{vn}{M}\right)\right) \right|^2 \qquad (13)$$

where (u,v) are spatial frequencies.

It is well known that this estimate is a non-consistent estimate of the power spectrum. For example, when the samples from a Gaussian white noise process are used, the periodogram
5 estimate has a variance that is proportional to the variance of the white noise process.

One approach to variance reduction is to segment the data, such as in non-overlapping blocks, where the spectrum is estimated in each block, using this periodogram estimator,
10 and obtaining the final estimate by averaging the periodograms of the blocks. In this manner, the variance is decreased by a factor equal to the number of blocks. Of course, this is at the expense of frequency resolution.

In the following, an iterative process is suggested for
15 estimating the dispersion matrix, which estimate is more sensitive to the anisotropies reflected in the low frequency parts of the orientation of the texture.

Algorithm 3   The dispersion matrix of the approximating Gaussian is estimated iteratively in the following way:

20   1. $\Sigma_0 = I$
         2. $i = 1$
         3. repeat
              3a. Estimate the dispersion:

$$\Sigma_i = \begin{pmatrix} \sigma_u^2 & \sigma_{uv} \\ \sigma_{uv} & \sigma_v^2 \end{pmatrix} \qquad (14)$$

where

$$\hat{\sigma}_u^2 = \sum_u \sum_v u^2 p(u, v) w(u, v) \tag{15}$$

$$\hat{\sigma}_v^2 = \sum_u \sum_v v^2 p(u, v) w(u, v) \tag{16}$$

$$\hat{\sigma}_{uv} = \sum_u \sum_v uv p(u, v) w(u, v) \tag{17}$$

and

$$w(u, v) = (u, v) \sum_{i-1}^{-1} \binom{u}{v} \tag{18}$$

```
    3b.  i = i-1
   until ||Σᵢ - Σᵢ₋₁||ₘₐₓ < δ
```

From both these techniques, the principal direction of the
5 power spectrum may be found using:

$$\alpha = \cos^{-1}\left(\frac{\sigma_{uv}}{\sqrt{\sigma_{uv}^2 + (\lambda_i - \sigma_u^2)^2}}\right) \tag{19}$$

This principal direction may be used to find the ellipse with
the smallest possible area, containing a fixed fraction of
the energy of the original (non-weighted) power spectrum. The
ellipse, rotated with the angle α around the origin, is
10 expressed in polar coordinates:

$$R(\theta)^2 = \frac{a^2 b^2}{b^2 \cos^2(\theta - \alpha) + a^2 \sin^2(\theta - \alpha)} \tag{20}$$

where a and b are the semi-major and semi-minor axis,
respectively, and where the above-mentioned λ's are the
eigenvectors.

In the present Example, the semi-major and semi-minor axes
15 may be found using the following scheme:

Algorithm 4   The steps outlined below are used to estimate
the semi-major and semi-minor axis in the ellipse with the
smallest possible area, containing a given fraction of the
spectral energy. The angle with which this ellipse should be
5 rotated around the origin is found as outlined above.

   1. Start with the semi-minor and semi-major axis suffi-
       ciently small, e.g., a = b = 10.

   2. Increase a and b with one, and calculate the fraction
       of energy in each ellipse (rotated with the angle α
10   around the origin).

   3. The ellipse with the largest fraction of energy is
       chosen.

   4. Repeat the steps 2 and 3 until the requested fraction
       of energy is reached.
15

The features considered here are the estimated values: $\hat{a}$, $\hat{b}$,
$\hat{a} \cdot \hat{b}$, $\hat{b}/\hat{a}$ as well as the features λ_1, λ_2, λ_2/λ_1, $\rho = \sigma_{uv}/\sigma_u \sigma_v$,
σ_v^2/σ_u^2, and:

$$\cos^{-1}\left(\frac{\sigma_{uv}}{\sqrt{\sigma_{uv}^2 + (\lambda_j - \sigma_u^2)^2}}\right) \tag{21}$$

$$\frac{|\sigma_u^2 - \sigma_v^2|}{\sqrt{(\sigma_u^2 - \sigma_v^2)^2 - 4\sigma_{uv}^2}} \tag{22}$$

$$\sum_u \sum_v (u^2 + v^2) p(u, v) \tag{23}$$

$$-\sum_u \sum_v p(u, v) \log(p(u, v)) \tag{24}$$

In Fig. 13, the estimated ellipse containing 70% of the
20 energy (and the direction) is shown for a 'normal' patient.
    In Fig. 14, the 70% ellipse is shown for an osteoporotic

patient. Clearly, the frequency content for the osteoporotic
patient is a lot more low-frequent. This means that the
energy is concentrated near the centre of the image and,
consequently, the areas of the ellipses are very different
5   although they contain the same fraction of energy.

Spatial Interaction Models

Above, it is described that a powerful set of features may be
extracted in the spatial frequency domain. However, the
performance of features extracted in the frequency domain
10   depend heavily on the spectral estimator used. The
periodogram is a non-consistent spectral estimator. This
problem may be overcome by segmenting the data in non-
overlapping segments, estimating the periodogram in each
segment and finally averaging over these periodograms.

15   The variance reduction is directly proportional to the number
of segments. However, this is at the expense of frequency
resolution.

In the following, we will consider two types of causal
Simultaneous AutoRegressive (SAR) models to obtain parametric
20   spectral estimates; the Non-Symmetrical Halfplane (NSHP)
model and the Quarter-Plane (QP) model.

Assume a wide sense stationary, zero mean, stochastic process
defined on a rectangular grid of pixel sites $\Omega = \{s=(s_r,s_c):$
$0 \le s_r \le M,\ 0 \le s_c \le N\}$, obeying a SARMA model defined as:

$$y_s + \sum_{r \in N_{AR}} \phi_r y_{s-r} = \epsilon_s + \sum_{r \in N_{MA}} \theta_r \epsilon_{s-r} \qquad (25)$$

25   where $r=(r_r,r_c) \in N_{AR}$ or N_{MA}. N_{AR} and N_{MA} are the regions of
support for the parameter arrays $\{\phi\}$ and $\{\theta\}$, respectively.
We also refer to these sets a neighborsets which, in some
sense, defines the order of the model.

The innovation process ϵ_s is assumed to be an IID $N(0, \Sigma_\epsilon^2)$ or Gaussian *white noise* sequence. If $N_{MA} = \emptyset$, we have a pure SAR model, and if $N_{AR} = \emptyset$, we have a pure SMA model.

In the following, we will focus on pure autoregressions, for
5 the following reasons: The use of mixed SARMA models would probably give more parsimonious models, but the models required to capture the nature of the considered texture are of a such low order that parsimony in not really an important issue. It also turns out that the important feature presently
10 is the shape of the spectrum in terms of e.g. peak locations. Also, the LS estimator for the pure SAR model is a set of linear equations, whereas non-linear optimization is required in order to obtain estimates of mixed SARMA models.

The (non-normalized) spectral density function is given as
15 the squared modulus of the frequency response function multiplied by the noise variance:

$$P_y(f) = \sigma_\epsilon^2 \frac{\left|1 + \sum_{r \in N_{MA}} \phi_r \exp(-2\pi i \cdot r^T \cdot f)\right|^2}{\left|1 + \sum_{r \in N_{AR}} \theta_r \exp(-2\pi i \cdot r^T \cdot f)\right|^2} \tag{26}$$

$$= \sigma_\epsilon^2 \frac{\left(1 + \underline{\theta}^T \underline{C}(N_{MA})_f\right)^2 + \left(\underline{\theta}^T \underline{S}(N_{MA})_f\right)^2}{\left(1 + \underline{\phi}^T \underline{C}(N_{AR})_f\right)^2 + \left(\underline{\phi}^T \underline{S}(N_{AR})_f\right)^2}$$

where the spatial frequencies $(f_r, f_c) = f \epsilon \Omega_f$, and

$$\Omega_f = (f = f_r, f_c) = \left(-\frac{1}{2} - \frac{r}{M}, -\frac{1}{2} + \frac{c}{M}\right) : (r, c) \in \Omega \tag{27}$$

The vector notation is defined as:

$$\underline{\phi} = \underline{col}[\phi_r, r \in N_{AR}] \tag{28}$$

$$\underline{\theta} = \underline{col}[\theta_r, r \in N_{MA}] \tag{29}$$

$$\underline{C}(N.)_f = \underline{col}[\cos(\omega(f,r)), r \in N.] \tag{30}$$

$$\underline{S}(N.)_f = \underline{col}[\sin(\omega(f,r)), r \in N.] \tag{31}$$

$$\omega(f,r) = 2\pi(r_r \cdot f_f + r_c \cdot f_c) \tag{32}$$

So far, the question of causality has not been addressed. In
two dimensions, the notion of causality is not natural.
Abandoning causality, however, leads to a number of
difficulties, one of them being that the Least Squares
5   estimator of the parameters is no longer consistent. Hence,
it has become popular to impose an artificial directionality
on the image, thus obtaining a causal model (in fact,
recursively computatable is a more correct term).

The two types of causal models typically considered in the
10   literature are the Quarter Plane support models (QP) and the
Non-Symmetrical HalfPlane support models (NSHP). In fig. 21,
parametric estimates using the NSHP model are illustrated. It
is seen that the spectrum is slightly elongated in a certain
direction, when compared to the corresponding periodogram
15   estimate seen in Fig. 22. This phenomenon is due to
directional bias which is an effect that is even more
pronounced for the QP mode. In order to solve this problem, a
Weighted QP (WQP) estimator has been proposed:

$$P_{AV}(f_r, f_c) = \frac{2}{\dfrac{1}{p_{++}(f_r, f_c)} + \dfrac{1}{p_{-+}(f_r, f_c)}} \tag{33}$$

where the subscripts ++ and -+ simply refer to the considered
20   quadrant, i.e. the first and the second quadrant. This
parametric estimator is widely considered to be among the
best parametrical spectral estimators, but it suffers from
the drawback that it has no model interpretation.

In fig. 23, a WPQ estimate is illustrated in which no
25   directional bias is seen.

Using these estimates, features of the type described above, that is: λ_1, λ_2, λ_2/λ_1, $\rho = \sigma_{rc}/\sigma_r\sigma_c$, σ_c^2/σ_r^2, and:

$$\alpha = \cos^{-1}\left(\frac{\sigma_{rc}}{\sqrt{\sigma_{rc}^2 + (\lambda_i - \sigma_r^2)^2}}\right) \tag{34}$$

$$\frac{|\sigma_r^2 - \sigma_c^2|}{\sqrt{(\sigma_r^2 - \sigma_c^2)^2 - 4\sigma_{rc}^2}} \tag{35}$$

$$\sum_{f_r}\sum_{f_c}(f_r^2 + f_c^2)p(f_r, f_c) \tag{36}$$

$$-\sum_{f_r}\sum_{f_c}p(f_r, f_c)\log(p(f_r, f_c)) \tag{37}$$

may be used.

Also, as α describes the principal orientation of the
5   approximating Gaussian, this direction may be used to find
the above-mentioned energy ellipses. Thus, also the semi-
major and semi-minor axes of these ellipses $\hat{a}$ and $\hat{b}$,
respectively as well as the features $\hat{a}\cdot\hat{b}$, $\hat{b}/\hat{a}$ may be used.

Extraction of features relating to periodicity

10   An alternative method of deriving features from the
preprocessed image of Fig. 6 is to again subject this image
to the two dimensional Fourier transformation and extract the
Fourier power spectrum (the periodogram spectrum).

It is presently preferred that the resolution of the image is
15   reduced using a Gaussian pyramid, thus, preserving as much of
the information as possible in the high resolution prior to
the Fourier transform.

Feature Extraction

It is not surprising that the power spectrum comprises peaks
20   corresponding to periodicity of the vertical trabeculae. It
is, however, fortunate that also peaks - however small -

corresponding to a periodicity of the horizontal trabeculae
may be discerned from the power spectrum.

Information relating to the density of trabeculae, their
thickness and the distance between them may be extracted from
5   the height of these peaks relating to the periodicities, the
total area under these peaks and/or the "width" thereof.

At present, it is preferred not to extract the peak positions
from the Fourier power spectrum, as the periodogram or the
power spectrum are very noisy due to the fact that the
10   periodogram estimator of the power spectrum is non-
consistent. Instead, a combined algorithm is preferred, where
the parametric spectrum is used to identify these peak
positions, and the smoothed periodogram is used to estimate
the associated energy etc.

15   In the power spectrum, a total of four peaks are typically
present - or more precisely, only two peaks, as the
parametric spectrum is symmetric. A line is drawn through the
two largest peaks (which relate to the vertical trabeculae)
through the DC-value. From the middle of. this line, a line is
20   drawn perpendicularly thereto also through the DC-value. It
is inherent from the model that the peaks of the horizontal
trabeculae are positioned perpendicularly to those of the
vertical trabeculae. The maxima on the new line will
correspond to the peaks of the horizontal trabeculae.

25   This method is preferred in order to be independent and
insensitive to any rotation of the image.

Smoothing of the spectrum may be performed using a kxk
kernel, such as a 5x5 kernel using, e.g., a mean filter, a
median filter, a Gaussian filter etc.

30   From this spectrum, the peak heights, the volume under the
peaks a.s.o. may be determined and used in the prediction of
the bone quality.

In addition, it is contemplated that also the curvature of the peaks in the parametric power spectrum may be used as a predictor of bone quality, as this curvature also relates to deviations of the periodicity.

5 **EXAMPLE 2: Study of feature performance**

A data set was used to investigate different image features and compare their performance. Radiographic images were obtained from 97 individuals and each image was ranked by experienced radiologists. The analysis of this data set is

10 described in the following.

Each patient was assigned the score +1 if the radiologist considered the patient to be 'normal' and the score -1 in case of accelerated bone loss (osteoporotic). The four radio- logists agreed upon the diagnosis in 52 cases, and only these

15 are used in this preliminary study. In this study of feature performance, a general linear model with the score as response variable and age, sex and textural features as explanatory variables is used. Furthermore, rigorous statis- tical tests of the significance of the individual features is

20 performed using a backwards elimination procedure.

The features used have been described above, and are all based on first, second and third order statistics measured on transforms of the projected trabecular pattern (PTP) or fitted ellipses on the Fourier power spectrum of the restored

25 images.

The fitted models are of the type

$$s_i = \beta_0 + \beta_1 age_i + \beta_2 sex_i + \beta_3 f_{1,i} + \cdots + \epsilon_i \qquad (38)$$

where s_i is the score of the i'th patient, age_i the age of the i'th patient, sex_i the sex of the i'th patient (+1: Male, -1: Female in order to make both sexes contribute equally to

the mean) and $f_{j,i}$ the j'th image feature of the i'th patient. It is assumed that ϵ is i.i.d. gaussian white noise. Under this assumption, the LS estimates are equal to the ML estimates. Test statistics are calculated for each parameter
5 in the model. Using a backwards elimination approach, the least significant parameter of the model is eliminated, and the model is subsequently re-estimated with the remaining parameters. This is continued until no more parameters can be eliminated from the model.

10 *Features based on the projected trabecular pattern*

Out of 12 image features, 9 were eliminated using the back- wards elimination procedure. The order in which they were eliminated is summarized in the table below:

Feature number	Feature name	1	2	3	4	5	6	7	8	9
1*	μ_D									
2	σ_D					•				
3³	cv_D									
4	γ_D			•						
5	μ_S						•			
6*	σ_S									
7	cv_S	•								
8	γ_S				•					
9	μ_M							•		
10	σ_M									•
11	cv_M		•							
12	γ_M								•	

15 The boldfaced features marked with an asterisk are signifi- cant parameters that could not be eliminated.

The resulting model is given by

$$s_i = \beta_0 + \beta_1 age_i + \beta_2 sex_i + \beta_3 \mu_{D,i} + \beta_4 cv_{D,i} + \beta_5 \sigma_S + \epsilon_i \qquad (39)$$

A summary of the resulting model is given below:

```
Call: lm(formula = score[idx4] ~
                   age + sex[idx4] + f[idx4, 1] + f[idx4, 3]
                   + f[idx4, 6])
```

Residuals:

5
	Min	1Q	Median	3Q	Max
	-3.755	-0.8549	-0.06046	0.7199	3.854

Coefficients:

	Value	Std. Error	t value	Pr(>|t|)
(Intercept)	50.2650	12.2399	4.1067	0.0002
age	-0.0995	0.0141	-7.0427	0.0000
sex[idx4]	1.1937	0.2579	4.6281	0.0000
f[idx4, 1]	-11.7739	2.3699	-4.9681	0.0000
f[idx4, 3]	-37.2419	11.0728	-3.3634	0.0016
f[idx4, 6]	2.7775	1.2370	2.2454	0.0297

15 Residual standard error: 1.746 on 45 degrees of freedom
Multiple R-Squared: 0.7516

Correlation of Coefficients:

	(Intercept)	age	sex[idx4]	f[idx4,1]	f[idx4,3]
age	0.0063				
sex[idx4]	-0.1329	0.2430			
f[idx4, 1]	-0.6991	-0.1573	-0.0231		
f[idx4, 3]	-0.9837	-0.0538	0.1220	0.7305	
f[idx4, 6]	-0.0287	0.1205	0.1072	-0.6269	-0.0918

Most of the explanatory effect is contained in the age and
25 the sex. The rest of the variability (approximately 16%
point) is explained by the textural features. It may be
desired to transform some of the features, or even derive new
ones.

From the above, it may be concluded that the considered
30 statistics measured on at least the distance transform and
the star area of the projected trabecular pattern, are quite

strong features. This investigation, however, does not sug-
gest the maximum distance transform as an optimal feature.

Fourier Features

In the following, four features extracted from the power
5   spectrum will be considered. The only feature eliminated from
this set of features is the length of the semi-major axis
(â). This is in good agreement with what would be expected,
as the erosion of the trabecular structure in osteoporotic
patients is mainly in the vertical direction. The performance
10 of the resulting model is comparable to the results obtained
using features based on the distance transform.

Again the data were analyzed in the statistical software
package *Splus*, and the following output was obtained for the
resulting model:

15 Residuals:

Min	1Q	Median	3Q	Max
-2.852	-1.114	-0.3153	0.6817	4.854

Coefficients:

	Value	Std. Error	t value	Pr(>|t|)
20 (Intercept)	8.1977	2.9152	2.8120	0.0073
ages[idx4,2]	-0.1086	0.0153	-7.1036	0.0000
sex[idx4]	1.2674	0.2711	4.6747	0.0000
freq[idx4,2]	8.6433	2.5788	3.3516	0.0016
freq[idx4,3]	-0.2102	0.0660	-3.1845	0.0026
25 freq[idx4,4]	-88.6948	24.0649	-3.6857	0.0006

Residual standard error: 1.843 on 45 degrees of freedom
Multiple R-Squared: 0.7232

Correlation of Coefficients:

	(Intercept)	ages[idx4,2]	sex[idx4]	freq[idx4,2]	freq[idx4,3]
ages[idx4,2]	0.0165				
sex[idx4]	0.0103	0.2150			
freq[idx4,2]	-0.2471	-0.1272	0.1435		
freq[idx4,3]	0.2189	0.1303	-0.1491	-0.9972	
freq[idx4,4]	0.1145	0.0866	-0.1543	-0.9880	0.9845

Thus, from the results of the above it may be seen that a
Multiple Correlation Coefficient better than 0.7 may be
obtained using only either the features extracted from the
power spectrum or the features extracted from the PTP; only
part of the features offered by the method of the invention.
Thus, it is contemplated that even higher Multiple Correla-
tion Coefficient may be expected when these groups of fea-
tures are combined in the estimation procedure. In this
connection it should be mentioned that Multiple Correlation
Coefficients of this size are quite satisfactory.

**EXAMPLE 3: The MORSE Estimator for Mixed Non-causal SARMA
Models**

The concept of texture is widely recognized as being of great
importance in many fields of application, such as, e.g.,
medical imaging, industrial quality inspection and remote
sensing. Visual properties of a given texture are, however,
not very tangible and many attempts has been made to extract
good and meaningful features in order to describe such prop-
erties.

One such approach is to model the spatial correlation struc-
ture using texture models. The two mainstream types of models
are the Gaussian Markov Random Field (GMRF) models and the
Simultaneous Auto-Regressive Moving Average (SARMA) models.
The latter type of models is an attempt to extend the very
powerful ARMA models (known from time-series analysis and 1-D
signal processing) to two dimensions.

Whereas 1-D signals are inherently causal, this is not a natural constraint in two dimensions. Abandoning causality, however, introduces severe problems in important modelling steps as identification and estimation. Therefore, it is very
5   popular to impose an artificial directionality on data and thereby obtaining consistent estimates by minimizing the sum of squared estimation errors - i.e. Least Squares estimates.

The analysis of non-causal SARMA models has been severely constrained, mainly due to the fact that the non-consistency
10   of the LS estimator forces one to consider a very complicated Likelihood function. As a consequence, the analysis has been concentrated solely on pure SAR models. The toroidal ML estimator and an approximative ML estimator has been formu-lated for pure SAR models. It can be shown that the perform-
15   ance of the approximative estimator may not be adequate when the considered textures is close to non-stationarity.

Considering the exact ML estimates for toroidal SAR models will, in general, give very good results. It is shown, how-ever, that the likelihood function is extremely rippled in
20   the vicinity of non-stationarity. This will, in many cases, cause the optimization routine to get 'caught' in a sub-optimal solution. This problem may indeed be serious as visual textures are often characterized by a strong positive correlation structure yielding estimates close to non-statio-
25   narity.

Another problem, which is related to the Maximum Likelihood estimator and the traditional Maximum Entropy estimators, is that these tend to overemphasize the high-frequency content of the considered.

30   Thus, a new, entropy based, estimator is introduced. Instead of maximizing the entropy of the associated model spectrum (as in MEM spectral estimation introduced in "A new algorithm for two-dimensional maximum entropy power spectrum estima-tion" Lim, J. S. & Malik, N. A. (1981) IEEE Transactions on

Acoustics, Speech and Signal Processing, 29, 401-413), the
entropy of the residual spectrum is maximized. This estimator
is named the MORSE estimator (Maximum Of Residual Spectral
Entropy). This estimator is well behaved, even close to
5   non-stationarity, which makes it much simpler to perform the
non-linear optimization of the involved objective functional
(w.r.t. the parameters). It is possible to write the objec-
tive functional for mixed SARMA models (i.e. including Moving
Average parts) and obtain very good estimates. To the best of
10   our knowledge there are no results in the literature regard-
ing inference in non-causal SARMA models.

The maximization of the residual spectral entropy seems,
intuitively, to be a reasonable criterion as the underlying
assumption of the simultaneous models is that the innovation
15   process is white. It is obvious that the optimality of a
given model is closely related to the chosen criterion of
optimality, and the choice of entropy is by no means the only
one to be imagined. Note that no assumptions are made
concerning the driving noise (innovation process ????)
20   sequence. We only require it to have a symmetrical
distribution.

The non-causal SARMA model

Consider a wide sense stationary, zero mean bilateral SARMA
process sampled on a square M×M grid of pixels $s=(r,c)\epsilon\Omega$

$$y_s + \sum_{r\in N_{\mu}} \phi_r y_{s-r} = \epsilon_s + \sum_{r\in N_{\mu}} \theta_r \epsilon_{s-r} \qquad (40)$$

25   where $r=(r_1,r_r) \epsilon$ N. and N. defines the *order* of the model.
The only assumption that is made about the innovation process
{y.} is that it is independent identically distributed random
variables with a *symmetrical* density.

Contrary to the GMRF models, the bilateral SARMA model does not have to be symmetrical, but opposite neighbours must be associated with identical parameters (i.e. $\phi_r = \phi_{-r}$. This is necessary to ensure the identifiability of the parameters.
5   For the sake of simplicity, the following is restricted to consider only symmetrical models.

In order to facilitate the notation when it is desired to be specific about the *order* of the model, the notation outlined in the following definitions is introduced:

10   *Definition 1*   A rectangle with side lengths 2a+1 and 2b+1, rotated by an angle α around the origin is denoted $R(a,b,\alpha)$. Now the following is defined

- $R(a,b) = R(a,b,0)$
- $R(a) = R(a,a,0)$

Definition 2   An ellipse with semi-major axis a and semi-minor axis b, rotated by an angle α around the origin is
15   denoted $E(a,b,\alpha)$. The following is defined

- $E(a,b) = E(a,b,0)$
- $E(a) = E(a,a,0)$

Thus, the *order* of a given model may be defined in terms of these geometrical shapes as, e.g., SARMA(E(1),E(1)) which means that the auto-regressive part, as well as the moving average part, is the four nearest neighbours.

20   If the bilateral model is considered, the stationarity condition is greatly weakened; all that is required is that no poles of the transfer function falls *on* the unit circle:

$$\left\{ 1 + \sum_{(m,n)\in N_{AR}} \phi_{m,n} z_r^{-m} z_c^{-n} \neq 0 \right\} \tag{43}$$

for all $|z_r| = 1$ and $|z_c| = 1$.

The transfer function is given as the 2-D z-transform of the impulse response function.

$$H(z_r, z_c) = \frac{X(z_r, z_c)}{E(z_r, z_c)} = \frac{1 + \sum_{(k,l)\in N_{MA}} \theta_{k,l} z_r^{-k} z_c^{-l}}{1 + \sum_{(k,l)\in N_{AR}} \phi_{k,l} z_r^{-k} z_c^{-l}} \tag{44}$$

and the frequency response function is obtained as the 2-D
5   Fourier transform of the impulse response function

$$\mathcal{H}(f(s)) = \frac{\left(1 + \Theta_{MA}^T C(N_{MA})_{f(s)}\right)}{\left(1 + \Theta_{AR}^T C(N_{AR})_{f(s)}\right)} \tag{45}$$

where

$$\tag{46}$$

$$f(s) = \left(\frac{r}{M} - \frac{1}{2}, \frac{c}{M} - \frac{1}{2}\right)^T$$

is the spatial frequency and

$$\begin{aligned}
\Theta_{MA} &= col[\theta_r, r \in N_{MA}] \\
\Theta_{AR} &= col[\phi_r, r \in N_{AR}] \\
C(N.)_{f(s)} &= col[\cos(2\pi f(s)^T r), r \in N.]
\end{aligned} \tag{47}$$

In time-series analysis and signal processing, the successful
use of ARMA models for spectral estimation has promoted an
10 interest in the extension of these methods to two dimensions.

As for ARMA models, the 2-D parametric spectrum is propor-
tional to the squared magnitude of the frequency response:

$$S(f(s)) = \sigma_\epsilon^2 |\mathcal{H}(f(s))|^2 \tag{48}$$

where σ_ϵ^2 is the variance of the innovation sequence.

Using this approach, the problem of spectrum estimation
5 becomes one of fitting an appropriate model to the observed
data. Mostly, parametric spectral estimation in 2-D has been
attempted using unilateral models. This typically leads to
directional bias. By using a bilateral model, this particular
problem should be solved, provided a practically applicable
10 estimation principle is provided. Our preliminary results
show that the MORSE estimation principle is a very useful
tool for obtaining parametric spectral estimates without
directional bias.

Different approaches have been made in order to obtain esti-
15 mates for the non-causal SAR model. There have, to the best
of our knowledge, been no results regarding estimation of
mixed non-causal SARMA models. Even for the pure SAR model
the estimation of the parameters is not a simple problem.
Below, different estimators for the non-causal SAR model will
20 be illustrated and their shortcomings discussed.

The Non-causal (or bilateral) Simultaneous Auto-Regressions
(SAR) models, sometimes referred to as NCSAR, were originally
introduced by P. Whittle in "On stationary processes in the
plane". Biometrika, 41, 343-449. The problem of non-consist-
25 ency of the LS estimator is addressed in this paper, and a
large sample approach based on spectral methods was pres-
ented. First, this method will be of use only for very simple
models and secondly, many practical situations involve small
samples for which the discounting of edge effects may not be
30 negligible. In order to illustrate how the non-consistency of
the LS estimator affects the estimates, a simple experiment

is carried out. For an isotropic nearest neighbour model, 100
realizations are generated for different parameters. In each
case, the parameters are estimated (as if the model was
anisotropic). In Fig. 15, the average of the estimated para-

5   meter is plotted versus the 'true' parameter (i.e. the para-
meter with which the texture was simulated). It is seen that
the LS estimator *does not* provide satisfactory estimates. In
fact, the order of magnitude is off by a factor two in many
cases.

10   Kashyap, R. & Chellappa, R. proposed an approximation to the
exact (toroidal) ML-estimator in "Estimation and choice of
neighbours in spatial interaction models of image", IEEE
Transactions on Information Theory, 29(1), 60-72. The approx-
imation is based on a Taylor-series expansion of the deter-

15   minant of the Jacobian (which becomes block circulant with
circulant blocks under the torus assumption). Only first- and
second-order parts (in the parameters) are included. The
improvement of the results is definitely vast, as shown in
Fig. 16 where the above experiment is repeated. Nevertheless,

20   as the bias is very pronounced close to non-stationarity, it
is seen that this estimator may not be adequate in many
practical situations where the textures tend to lie close to
non-stationarity, and it is highly preferred to obtain a more
suitable estimator not having these disadvantages.

25   Grunkin investigated the exact (toroidal) ML-estimator in "On
The Analysis of Image Data Using Simultaneous Interaction
Models" in IMSOR, ph.d thesis # 67, Institute of Mathematical
Statistics and Operations Research, Technical University of
Denmark, Lyngby, 223pp. The likelihood function involved is

30   complicated and computationally very expensive. Also, the
likelihood function is extremely rippled in the vicinity of
non-stationarity as shown in Fig. 17. Whether the non-linear
optimization routine is 'caught' in a sub-optimal solution or
not is very much dependent upon the initial guess and the

35   parameters of the optimization algorithm (such as, e.g., step
length). Thus, it may take several re-estimations to be

convinced that the correct solution is found. This, of
course, is merely a technical problem, and in the simple
experiment described above, these problems can be overcome
and the exact (toroidal) ML-estimates yield very good results
5   as shown in Fig. 18.

The MORSE estimator

As mentioned above, the non-consistency of the LS estimator
is leads to non-sensical results. The practical application
of the exact toroidal ML estimator will, in many cases, be
10   limited, as the likelihood function tends to be extremely
rippled in the vicinity of non-stationarity. Thus, it may
require several re-estimations to ensure that the 'true'
optimum is found. Also, as pointed out earlier, the ML esti-
mator may overemphasize the high-frequent content of the
15   texture. In addition, the computational load involved in
obtaining estimates for mixed SARMA models using the ML
estimation principle is prohibitive for all practical
purposes.

The approach taken here is to consider the spectral content
20   of the residuals. Finally, it will probably be extremely
difficult to obtain ML estimates of mixed non-causal SARMA
models.

In this Example, a novel estimator is described that gives
very good estimation results, has a response surface that (in
25   our experience) is very well behaved and allows for inference
in mixed SARMA models.

As the underlying assumption is that the residuals should be
white, i.e. uncorrelated, all frequencies should be represen-
ted, with the same weight, in the spectrum of the residual
30   process. If the residual spectrum is normalized, the entropy
of the residual spectrum obtains its maximum when the spec-
trum is as flat as possible. This observation is the basis of
the Maximum Of Residual Spectral Entropy (MORSE) estimator.

Consider again the difference equation defining the system:

$$y_s + \sum_{r \in N_{r}} \phi_r y_{s-r} = \epsilon_s + \sum_{r \in N_{a}} \theta_r \epsilon_{s-r} \qquad (49)$$

The output can be viewed as the convolution of the innovation process with the impulse response of the system. Thus, in the frequency domain, the following representation is found:

$$Y(f(s)) = \mathcal{H}(f(s)) \cdot E(f(s)) \qquad (50)$$

5   where $Y(f(s))$ is the Fourier transform of the output, $E(f(s))$ is the Fourier transform of the (non-observable) innovation process and $\mathcal{H}(f(s))$ is the Fourier transform of the impulse response function, which is also known of the frequency response function.

10 Using equation (50), the power spectrum of the innovation process may be expressed in terms of the power spectrum of the observations and the parametric spectrum (assuming that the parameters are known). Thus it is found that:

$$|E(f(s))|^2 = \frac{|Y(f(s))|^2}{|\mathcal{H}(f(s))|^2} = |Y(f(s))|^2 \frac{\left(1 + \Theta_{AR}^T C(N_{AR})_{f(s)}\right)^2}{\left(1 + \Theta_{MA}^T C(N_{MA})_{f(s)}\right)^2} \qquad (51)$$

A normalization function depending upon the observations and
15 the parameters may be defined:

$$N(\underline{y}, \underline{\Theta}_{AR}, \underline{\Theta}_{MA}) = \sum_{s(s)} |E(f(s))|^2 = \sum_{s(s)} \frac{|Y(f(s))|^2}{|\mathcal{H}(f(s))|^2} = M^2 \sigma_\epsilon^2 \qquad (52)$$

The parameters are subsequently found by maximizing the entropy of the residual spectrum.

Definition 3   The Maximum Of Residual Spectral Entropy
(MORSE) estimates are found by maximizing the entropy func-
tion $L(\underline{y}, \underline{\Theta}_{AR}, \underline{\Theta}_{MA})$ with respect to the parameters $\underline{\Theta}_{AR}$ and $\underline{\Theta}_{MA}$:

$$(\underline{\hat{\Theta}}_{AR}, \underline{\hat{\Theta}}_{MA}) = \arg \max_{(\underline{\Theta}_{AR}, \underline{\Theta}_{MA})} L(\underline{y}, \underline{\Theta}_{AR}, \underline{\Theta}_{MA}) \tag{53}$$

where

$$L(\underline{y}, \underline{\Theta}_{AR}, \underline{\Theta}_{MA}) = -\sum_{f(s)} \frac{|E(f(s))|^2}{M^2 \sigma_\epsilon^2} \log \frac{|E(f(s))|^2}{M^2 \sigma_\epsilon^2} \tag{54}$$

5

An estimate of the residual variance is obtained as

$$\hat{\sigma}_\epsilon^2 = N(\underline{y}, \underline{\hat{\Theta}}_{AR}, \underline{\hat{\Theta}}_{MA})/M^2 \tag{55}$$

Clearly, this function is strongly non-linear in the parame-
ters. The optimization may be carried out using, e.g., a
Quasi-Newton method. In this work, the IMSL implementation of
10   the BFGS method is applied.

Experimental results

As illustrated above, the exact (torus-)ML-estimates give
very good results. The problem here is of a more technical
nature. Firstly, the involved likelihood function (or objec-
15   tive functional) is extremely complicated and computationally
expensive to evaluate. Secondly, the likelihood function is
very rippled in the vicinity of non-stationarity.
Consequently any optimization-routine might easily 'get
caught' in a sub-optimal solution.

20   Above, important problems as centrality, consistency,
efficiency of the proposed estimator have not been addressed.

Obviously, questions as these are difficult to answer analytically due to the untractable form of the involved expressions. Below, these questions will be addressed empirically through simulation and estimation experiments.

5   *Estimation of pure SAR models*

In Fig. 19, the objective functional of the MORSE estimator is shown in the same region as the ML-estimator. It is clear that the objective functional of the MORSE estimator is much smoother - i.e. there are *no* ripples. It is our experience
10 that the objective functional of the MORSE estimator never exhibits ripples in parameter space - not even outside the admissible region. This makes the non-linear optimization a rather straight-forward task that can be undertaken automatically by most standard software packages.

15 The experiment carried out for the various estimators above in connection with Fig. 17 is also carried out for the MORSE estimator. The result is shown in Fig. 20, and it is seen that the results are very acceptable. Note that the variance *decreases* as non-stationarity is approached. This is due to
20 the fact that the poles in the transfer function are approached. Such poles (or near-poles) create sharp peaks in the objective functional and thereby a much smaller variance.

Estimation of mixed SARMA models

A major advantage of this approach is that an estimator for
25 mixed SARMA models is obtained 'for free'. In order to illustrate that good results are obtained for the mixed SARMA models as well, the following experiment is conducted. A set of parameters are chosen for a SARMA(E(1.0),E(1,o)) model. Furthermore, these parameters are chosen not too far away
30 from non-stationarity so that strong *positive* spatial auto-covariances are obtained. Now 100 simulations are carried out and the histogram of each parameter is plotted with the 'true' parameter marked as shown in Fig. 20.

Another test is one where 1000 realizations of size 64x64
pixels and 1000 realizations of size 128x128 pixels are
generated - also not too far from non-stationarity. For each
of these realizations, the MORSE estimator was used to obtain
5 an estimate of the model parameters. The empirical 95%-
confidence intervals are calculated for the mean of each
parameter. In fig. 24, it is seen that the known values of
the parameters fall nicely within these confidence intervals
further indicating that the estimator is central. It should
10 also be noted that the width of the confidence intervals
decrease as the size of the synthesized texture samples
increase. This indicates that the estimator is consistent.

Thus, it is seen that very satisfactory results are obtained
also for the mixed non-causal SARMA model.

15 *Distributional properties of the estimator*

It might intuitively be expected that the distribution of the
estimated parameters be Gaussian if the driving noise was
Gaussian. As this is hard to prove formally, this is made
probable through experiments. Histograms of the parameters,
20 estimated from the 1000 128x128 simulated textures described
above, are shown in Fig. 25. The hypothesis that the shown
histograms represent samples of Gaussian estimates will now
be formally tested using the χ^2 test. For each parameter, the
estimates are divided into K classes, where K is selected as
25 K = $1+3.3\log_{10}(N)$ (where N is the number of observations). In
order to make the test as strong as possible, the classes are
selected such that the expected number of observations is
equal in each class. This is done by generating the splits as
the $(i\cdot100/k)$%-quantile $(i=1,...,K-1)$. The test statistic is
30 now computed as:

$$Z = \sum_{i=1}^{K} \frac{(Obs_i - \frac{N}{K})^2}{\frac{N}{K}} \qquad (56)$$

Where Obs_i is the number of observations in the i'th class. This test statistic is distributed as $\chi^2(K-3)$ (since both mean and standard deviation should be estimated). The tests are summarized in the below table, where it is seen that the

5   distributional hypothesis is easily accepted for all parameters.

$\tau_i \in N$	θ_i	mean of θ_i	sdev of θ_i	Z	$P\{Z > \chi^2(8)\}$
$AR(-1,0)$	-0.22314	-0.22308	0.00757	5.44	0.709
$AR(0,-1)$	-0.12118	-0.12126	0.00808	6.94	0.543
$MA(-1,0)$	0.11535	0.11521	0.00772	7.512	0.483
$MA(0,-1)$	0.24066	0.24083	0.00759	6.038	0.643

Conclusion

The principle on which this estimator lies is intuitively

10   very appealing. The empirical results obtained for this estimator is, indeed, very promising. Using this estimator, also non-causal SARMA models may be considered.

EXAMPLE 4: Test of the presently preferred method

In the present example, a test was performed in order to

15   evaluate the applicability of the present method in the prediction of bone strength on the basis of X-ray pictures of the bone.

Data set

The data set consisted of 20 samples of the third lumbar

20   vertebrae harvested from cadaveric specimens each of which were exposed to X-ray irradiation in order to obtain an X-ray picture and a BMD measurement of each bone.

Subsequently, an anterior and a posterior core sample of trabecular bone was extracted from each bone, and the optimal

25   fracture load was determined for each of these samples using a three-point test setup as known per se.

The X-ray pictures were scanned with a spatial resolution of 600 lines per cm. In the final resolution, an area is selected centrally positioned between the positions of the drilled-out samples. The positions of the core samples may be 5 partly or fully comprised in the selected area.

It was decided to choose the mean optimal fracture load of the two core samples of a bone as the strength of the bone. This largely corresponds to the strength of the bone in the central part as determined by linear interpolation of the 10 strengths of the two samples. The results of the present test seems to confirm that this decision is reasonable.

Pre-processing of the image material

In order to have as good images as possible in the final, much smaller resolution, the scanned X-ray images had a large 15 spatial resolution (600 lines per centimetre).

The present images were so large that a scale reduction using a Burt-Adelson Gaussian pyramid was impossible due to the computer having too little memory. Thus, as a preliminary reduction was performed by firstly smoothing the image using 20 a 3x3 mean filter and subsequently discarding every other pixel in the image.

After this preliminary reduction, the image had a size reducible by the Burt-Adelson Gaussian pyramid to obtain the final resolution (150 lines per centimetre).

25 Subsequent to the reduction of the image, the image was background corrected by subtracting a 31x31 median filtered version of itself.

From the corrected image, a Region Of Interest (ROI) having a size of 256x256 pixels was selected. Preferably, this ROI was 30 selected close to the center of the bone due to the fact that a large gradient of the thickness of the trabeculae was

present close to the anterior and posterior ends of the bone.
This effect and the fact that the bone is rounded towards its
ends created a number of non-linear effects in the image
dynamics which cannot be dealt with in a trivial manner.

5   Having extracted the Region Of Interest, the image was
    filtered in order to remove high frequency noise. As the
    signal-to-noise relation of the present image was very high,
    the high frequency noise may be removed in a "gentle" manner:

```
    fourtr > fft.$$
10  htof -CR M < fft.$$ | powerpix -p 1.8 > mag.-$$
    htof -CR P < fft.$$ > pha.$$
    combine -pm pha.$$ < mag.$$ | inv.fourtr | htof -CR R | scale
    rm *.$$
```

    This manner is an alternative to the method of algorithm 1 on
15 pages 27 and 28, as, in this method, T=2 and p=1.8.

    From this pre-processed image, the Projected Trabecular
    Pattern (PTP) is extracted in the manner described above in
    connection with Algorithm 2. Substantially all features
    described in Example 1 were calculated.

20 *Statistical methods*

    It was attempted to construct a General Linear Model for
    predicting the ultimate strength. In this connection, it is
    imperative to identify the important parameters and eliminate
    the unimportant ones. As there are a large number of
25 variables and as only a small number of observations were
    evaluated, it was not possible to directly use a Backwards
    Elimination method as $(X_T X)$ typically will be singular in
    this situation. In addition, there is also the risk of
    eliminating the wrong variables. Therefore, in the following
30 a method is used which resembles a Forward Elimination method
    performed as follows:

1. Search through the list of possible features until the first significant feature is identified.

2. Continue the search until another significant feature is identified and included in the model.

5   3. Test whether previous features should be eliminated.

Steps 2. and 3. are repeated until all features have been investigated. Naturally, a level of significance should be decided for the described tests. In the present investigation, this level is chosen at p=0.10, as the amount

10 of data does not make a very conservative test possible.

It became clear that the optimal fracture load related exponentially to the parameters of the model, whereby the model was performed as a regression with the *logarithm* to the optimal fracture load as a dependent variable.

15 Choosing the parameters according to the above principle, only three significant parameters were found: â (See Algorithm 4), Formula (23) squared, and μ_S^2 (See Formula (3)).

In the following, these parameters are evaluated in two

20 models, one using age as a variable and one not using age.

Modelling without age

A General Linear Model not using age as a descriptive variable was made. This model will, thus, seek to predict the optimal fracture load on the basis of the extracted

25 structural indices. The result is summarized in the below program printout:

Residuals:

Min	1Q	Median	3Q	Max
-0.4327	-0.2409	0.03446	0.1625	0.5578

Coefficients:

	Value	Std. Error	t value	Pr(>|t|)
(Intercept)	11.2930	1.8815	6.0020	0.0000
$\hat{a}$	-70.8473	21.1912	-3.3432	0.0044
μ_S^2	-0.0287	0.0037	-7.8621	0.0000
(Formula 23)^2	143625.7515	53274.0853	2.6960	0.0166

Residual standard error: 0.2901 on 15 degrees of freedom

Multiple R-Squared: 0.8158

F-statistic: 22.14 on 3 and 15 degrees of freedom, the p-value is 9.17e-06

Correlation of Coefficients:

	(Intercept)	$\hat{a}$	μ_S^2
$\hat{a}$	-0.9873		
μ_S^2	-0.5412	0.4485	
(Formula 23)^2	0.4347	-0.5455	-0.1318

Explaining model:

$$F_{av}^{max}=\exp(-70.8473\cdot(Formula23)^2-0.0287\cdot\hat{a}$$
$$+143625.7515\cdot\mu_S^2+11.2930) \tag{57}$$

No.	log(Msrd)	log(Predicted)	Residual
238	4.574778	4.302492	0.272286112
240	4.259244	4.168912	0.090332350
242	4.516842	4.742086	-0.225244419
247	4.677491	4.800312	-0.122820941
250	3.508197	3.473737	0.034459077
254	4.070737	4.402031	-0.331293705
258	2.501764	2.864725	-0.362961146
259	3.724428	3.682320	0.042107301
265	4.443404	3.885623	0.557781393
267	5.382806	5.098572	0.284233332
269	4.099266	3.949321	0.149945096
279	4.434097	4.125558	0.308539021
280	3.844675	4.277384	-0.432709063
281	3.372283	3.310585	0.061698025
289	3.823039	3.808975	0.014063294
293	3.779999	3.604959	0.175040294
296	3.527713	3.784313	-0.256600239
298	3.896777	3.886981	0.009796051
313	4.397531	4.666183	-0.268651834

In Fig. 26 a plot of the logarithmic optimal fracture load against the predicted strength is illustrated. In this figure, the measurement points are represented by their number in the database.

5   At this point it is, naturally, interesting to know whether the BMD measurements performed on all samples may take part as a statistically significant feature contributing to increasing the multiple R-squared. The result may be seen from the below printout

10 Residuals:

Min	1Q	Median	3Q	Max
-0.4342	-0.2389	0.0385	0.1615	0.5598

Coefficients:

	Value	Std. Error	t value	Pr(>|t|)
(Intercept)	11.3316	2.2940	4.9397	0.0002
$\hat{a}$	-71.1532	23.9423	-2.9719	0.0101
$\mu_S{}^2$	-0.0288	0.0044	-6.5255	0.0000
Formula 23 squared	144161.1908	57644.4790	2.5009	0.0254
BMD	-0.0190	0.5953	-0.0319	0.9750

Residual standard error: 0.3002 on 14 degrees of freedom
Multiple R-Squared: 0.8158
F-statistic: 15.5 on 4 and 14 degrees of freedom, the p-value is 8.43e-05

25 Correlation of Coefficients:

	(Intercept)	$\hat{a}$	$\mu_S{}^2$	Formula 23 squared
$\hat{a}$	-0.9798			
$\mu_S{}^2$	-0.6661	0.5587		
Formula 23 squared	0.5070	-0.5949	-0.2583	
BMD	-0.5285	0.4009	0.5154	-0.2914

It is obvious that BMD is not a significant feature and that it can be eliminated from the model. Using BMD as the only descriptive parameter, a multiple R-squared of $R^2=0.2142$ is obtained indicating that BMD is a poor indicator of the
5   quality of trabecular bone. Thus, the aspects of fracture risk relating to trabecular bone are poorly described by BMD.

Modelling with age

Using age as a describing parameter, the following model is obtained:

10   Residuals:

Min	1Q	Median	3Q	Max
-0.3777	-0.1385	0.02544	0.1517	0.328

Coefficients:

	Value	Std. Error	t value	Pr(>|t|)
15 (Intercept)	11.8882	1.6616	7.1545	0.0000
$\hat{a}$	-68.3085	18.5326	-3.6858	0.0024
μ_S^2	-0.0236	0.0039	-6.1152	0.0000
Formula 23 squared	152951.1278	46677.8586	3.2767	0.0055
20 AGE	-0.0160	0.0067	-2.3827	0.0319

Residual standard error: 0.2533 on 14 degrees of freedom
Multiple R-Squared: 0.8689
F-statistic: 23.2 on 4 and 14 degrees of freedom, the p-value is 4.707e-06

25   Correlation of Coefficients:

	(Intercept)	$\hat{a}$	μ_S^2	Formula 23 squared
$\hat{a}$	-0.9658			
μ_S^2	-0.3585	0.4028		
30 Formula 23 squared	0.4408	-0.5378	-0.0617	
AGE	-0.1503	-0.0575	-0.5613	-0.0838

Explaining model:

$$F_{av}^{max}=\exp(-68.3085\cdot(Formula23)^2-0.0236\cdot\hat{a}$$
$$+152951.1278\cdot\mu_s^2-0.016\cdot AGE+11.8882)$$

(58)

No.	log(Msrd)	log(Predicted)	Residual
238	4.574778	4.293879	0.280898703
240	4.259244	4.262127	-0.002882869
242	4.516842	4.505306	0.011535494
247	4.677491	4.766867	-0.089375665
250	3.508197	3.413527	0.094669315
254	4.070737	4.435918	-0.365180333
258	2.501764	2.852028	-0.350263751
259	3.724428	3.625144	0.099283320
265	4.443404	4.238432	0.204971765
267	5.382806	5.273592	0.109213882
269	4.099266	3.964857	0.134408820
279	4.434097	4.106100	0.327997388
280	3.844675	4.032239	-0.187563938
281	3.372283	3.394572	-0.022288673
289	3.823039	3.797599	0.025439956
293	3.779999	3.610914	0.169084738
296	3.527713	3.829923	-0.302210802
298	3.896777	3.656788	0.239989248
313	4.397531	4.775257	-0.377726598

In Fig. 27 a plot of the logarithmic optimal fracture load
against the predicted strength is illustrated. In this
5   figure, the measurement points are represented by their
number in the database.

Discussion

From the result of the present example, it is clear that the
optimal fracture load of trabecular bone may be predicted
10   using only textural parameters - and even with a high
precision. Three image features are used: Formula 23 squared,
μ_s^2, and $\hat{a}$ describing the density of the horizontal
trabeculae (the thickest), the break down of the trabecular
structure, and the global trabecular density, respectively.
15   In addition, it is seen that neither sex nor BMD can add

information to the description obtained using the above three
image features.

However, it is seen that age is a significant parameter.
Including age in the model increases the multiple R-squared
5 to $R^2=0.8689$. It should be noted that the two extreme
observations (258 and 267) contribute quite a lot to the
value of R^2. Omitting these observations gives $R^2=0.7538$,
including age, which should still be regarded as a high
multiple R-squared.

10 However, as is described in connection with Algorithm 1, the
parameters used in restoring the image will a large effect on
the applicability of the features extracted from the
resulting image. In fact, using p=1.4 and T=4 instead of
p=T=2 in algorithm 1, the feature σ_M alone gives a R^2 of
15 0.92.

In Fig. 28, the correlation between σ_M and the logarithm to
the optimal fracture load is illustrated for a test based on
the picture and optimal fracture load - material described
above. Even if the extreme point in the lower right corner of
20 the figure is removed, a correlation of 0.88 is obtained.

Thus, a very large difference may be seen depending on the
actual manner of obtaining the PTP of the image.

CLAIMS

1. A method for estimating the bone quality of a vertebrate, on the basis of two-dimensional image data comprising information relating to the trabecular structure of at least a

5   part of a bone of the vertebrate, the image data being data obtained by exposing at least the part of the bone to electromagnetic radiation, the method comprising subjecting the image data to a statistical analysis comprising

-    a background correction procedure in which low frequent

10   intensity variations not related to the trabecular structure of the bone is reduced relative to image data related to the trabecular structure of the part of the bone,

-    an image manipulation and feature extraction procedure

15   wherein at least the local image intensity information as well as variation in the local intensity are utilized to extract information related to the trabecular structure of the part of the bone, the image manipulation and feature extraction procedure comprising

20   subjecting the image data to at least one of the following procedures:

(a)   obtaining an estimate of the parametric estimate of the power spectrum of the image data and extracting features relating to the energy

25   distribution of the parametric estimate,

(b)   obtaining, on the basis of image data on which a Fourier method has been used to emphasize the information in the image data relating to the trabecular structure, an estimate of a grey-level

30   co-occurrence matrix and extracting at least one feature on the basis of the estimated co-occurrence matrix,

(c)   obtaining an estimate of the projected trabecular pattern of the image data by using a Fourier

35   method to emphasize the information in the image data relating to the trabecular structure and

subjecting the manipulated image data to a
morphological operation, and extracting features
relating to the trabecular structure from the
estimated projected trabecular pattern,

5   (d)   obtaining, on the basis of a frequency analysis
of the image data, features relating to the
periodicity of the trabecular structure of the
part of the bone,

-          and an estimation procedure in which the bone quality of
10   the vertebrate is estimated on the basis of the derived
features and optionally other features related to the
bone or the vertebrate and a predetermined relationship
between the features and reference bone quality parame-
ters.

15   2. A method according to claim 1, wherein the electromagnetic
radiation is X-ray radiation.

3. A method according to any of the preceding claims, wherein
the image data is scanned from an X-ray film.

4. A method according to claim 3, wherein the resolution of
20   the X-ray film is at least 4 pairs of lines per centimetre,
such as at least 5 pairs of lines per centimetre.

5. A method according to claim 4, wherein the resolution of
the X-ray film is at least 10 pairs of lines per centimetre,
such as at least 25 pairs of lines per centimetre, preferably
25   at least 50 pairs of lines per centimetre.

6. A method according to claim 5, wherein the resolution of
the X-ray film is at least 100 pairs of lines per centimetre,
such as at least 250 pairs of lines per centimetre, preferab-
ly at least 500 pairs of lines per centimetre, such as at
30   least 600 pairs of lines per centimetre.

7. A method according to claim 3, wherein the scanning has
been performed at a resolution of at least 10 lines per cm.

8. A method according to claim 7, wherein the resolution is at least 25 lines per cm.

9. A method according to claim 8, wherein the resolution is at least 100 lines per cm, such as at least 200 lines per cm,
5 such as at least 250 lines per cm.

10. A method according to any of the preceding claims, wherein the background correction procedure comprises at least reducing or optionally removing low frequency information having a frequency significantly lower than the spacing of
10 the projected trabeculae.

11. A method according to claim 10, wherein information having frequencies half or less than the spacing of the projected trabeculae is at least reduced or optionally removed.

15 12. A method according to claim 11, wherein information having frequencies being a quarter or less than the spacing of the projected trabeculae is at least reduced or optionally removed.

13. A method according to claim 12, wherein information
20 having frequencies being a tenth or less the spacing of the projected trabeculae is at least reduced or optionally removed.

14. A method according to any of claims 10-13, wherein the background correction procedure comprises generating second-
25 ary image data as a result of performing a median filtering with a predetermined kernel size and subtracting this result from the original image data.

15. A method according to any of claims 10-13, wherein the background correction procedure comprises generating second-
30 ary image data as a result of performing a mean filtering

with a predetermined kernel size and subtracting this result
from the original image data.

16. A method according to any of claims 10-13, wherein the
background correction procedure comprises globally fitting a
5   two-dimensional polynomial to the image data and generating
background corrected image data on the basis of the residuals
of the fitting procedure.

17. A method according to claim 16, wherein the order of the
polynomial is at the most 15, such as at the most 10, prefer-
10 ably at the most 5.

18. A method according to claim 14 or 15, wherein the kernel
size is at the most 1/2 of the image data, such as at the
most 1/4 of the image data, preferably at the most 1/10 of
the image data, more preferably at the most 1/20 of the image
15 data.

19. A method according to any of the preceding claims, where-
in the parametric estimate of the power spectrum is estimated
by using a method selected from the group consisting of
direct methods, auto-covariance methods and parametric
20 methods.

20. A method according to claim 19, wherein the image data,
optionally weighted with a window, is subjected to a Fast
Fourier Transformation in order to generate the parametric
estimate.

25 21. A method according to claim 19, wherein the auto-
covariance function estimated on the basis of the image data,
optionally weighted with a window, is subjected to a Fast
Fourier Transformation in order to generate the parametric
estimate.

30 22. A method according to claim 19, wherein one of the
methods on the basis of which the parametric estimate is

obtained is chosen from the group consisting of: causal
Simultaneous Auto-Regressive Moving Average (SARMA) models,
non-causal SARMA models, Gaussian Markov Random Field models
and Maximum Entropy Spectral Estimates and wherein the order
5   of the model is identified, the parameters of the model are
estimated and the spectrum of the estimated model is gener-
ated.

23. A method according to claim 22, wherein the method on the
basis of which the parametric estimate is obtained, is a non-
10   causal SARMA model using an estimator according to claim 50.

24. A method according to any of the preceding claims, where-
in at least one feature is related to parameters of a contour
encompassing at least a predetermined percentage of the
energy of the power spectrum.

15   25. A method according to claim 24, wherein the contour is
determined by
     (a) defining a contour, in terms of one axes in each
         dimension, around the centre of the power spectrum, all
         points on the contour having substantially the same
20   distance to the centre of the power spectrum, and the
         contour encompassing less than the predetermined
         percentage of the energy of the power spectrum,
     (b) for each dimension of the data calculating the per-
         centage of the energy of the power spectrum encompassed
25   by a dilated contour in which the axis in the dimension
         in question is increased by a predetermined distance,
     (c) increasing the axis of the contour, in the dimension in
         which the increase in energy encompassed by the dilated
         contour is the largest, by the predetermined distance
30   and
     (d) repeating steps (b) and (c) until the percentage
         encompassed by the contour exceeds or equals the
         predetermined percentage.

26. A method according to claim 24 or 25, wherein the contour is ellipsoidal, optionally spherical.

27. A method according to claim 25 or 26, wherein the axis of the contour are orthogonal and are defined along principal
5   directions of the power spectrum.

28. A method according to claim 1, wherein procedure (c) is used and wherein the Fourier method comprises
- subjecting the image data to Fourier transformation,
- performing a subsequent mathematical transformation of
10   the Fourier transformed data,
- converting the transformed data back into the spatial domain.

29. A method according to claim 28, wherein the subsequent mathematical transformation is linear or non-linear.

15 30. A method according to claim 29, wherein the subsequent mathematical transformation is performed by raising the data to a power larger than 1, such as a power in the range of 1.1-10, preferably 1.5-4, such as about 2.0.

31. A method according to any of claims 28-30, wherein a
20   third mathematical transformation is performed in order to preserve only part of the magnitude information of the transformed data.

32. A method according to any of claims 28-31, wherein the emphasized information in the image data relating to the
25   trabecular structure is subjected to a grey-scale morphological operation.

33. A method according to claim 32, wherein the grey-scale morphological operation is a top-hat operation wherein all pixels fitting in the top-hat are assigned a value different
30   from a specified background pixel value.

34. A method according to claim 33, wherein the image data which has been subjected to the top-hat operation is thresholded so as to assign a foreground pixel value to the pixels having a pixel value different from the background pixel
5   value.

35. A method according to any of claims 32-34, wherein the image data which has been subjected to the grey-scale morphological operation is subjected to further noise reduction to substantially remove isolated single pixels and pixel
10   groups smaller than a predetermined threshold number of pixels having a pixel value different from the background pixel value.

36. A method according to any of claims 32-35, wherein an operation is performed comprising determining, for each
15   background pixel, the distance according to a given metric from the background pixel to the nearest foreground pixel, and wherein at least one feature is extracted from the result of the operation.

37. A method according to claim 36, wherein at least one
20   feature relates to a mean value and/or standard deviation and/or the coefficient of variation and/or skewness and/or kurtosis of the determined distances from all background pixels to the nearest foreground pixel.

38. A method according to any of claims 32-35, wherein an
25   operation is performed comprising determining a measure for each background pixel based upon determining the distance from the background pixel in a number of given directions in the image data to the nearest foreground pixel and at least one feature is extracted from the result of the operation.

30   39. A method according to claim 38, wherein at least one feature relates to a mean value and/or standard deviation and/or the coefficient of variation and/or skewness and/or

kurtosis of the determined measures for all background pixels.

40. A method according to claim 38 or 39, wherein the measure for each background pixel is a mean value and/or standard
5 deviation and/or the coefficient of variation and/or skewness and/or kurtosis and/or maximum distance of the determined distances in the given directions.

41. A method according to any of the preceding claims, wherein at least one feature related to the bone or to the
10 vertebrate, such as age and/or sex, and/or species, and/or race and/or the specific bone considered in the vertebrate, and/or an estimated Bone Mineral Density of the bone, and/or an estimated Bone Mineral Content of the bone, is included in the estimation procedure.

15 42. A method according to claim 41, wherein the Bone Mineral Density is estimated by including data from a reference object in the exposure of the bone to the electromagnetic radiation and where the Bone Mineral Density is estimated by correlating the absorption of the electromagnetic radiation
20 of the bone and of the reference object.

43. A method according to any of the preceding claims, wherein the estimation procedure is based on a statistical model, taking into account the correlation structure in the data set, so as to assign appropriate weights to the
25 significant features in accordance with the predetermined relationship.

44. A method according to any of the preceding claims, wherein the reference bone quality is an absolute or relative bone quality of bones for which image data have been
30 processed in accordance with any of the preceding claims.

45. A method according to claim 44, wherein the reference bone quality is determined on the basis of measurement of the

mechanical bone strength, and/or Bone Mineral Density
measurement, and/or on the basis of a Bone Mineral Content
measurement, and/or on the basis of a score of the bone
strength by a skilled radiologist.

5   46. A method according to any of the preceding claims,
wherein the predetermined relationship between the features
and reference bone quality parameters is established on the
basis of reference bone quality parameters and features
extracted according to any of the preceding claims.

10   47. A method according to claim 46, wherein the predetermined
relationship is defined in terms of a model taken from the
group consisting of: a General Linear Model, a Generalized
Linear Model, an Artificial Neural Network, a Causal
Probabilistic Net and Classification And Regression Trees.

15   48. A method according to any of the preceding claims,
wherein the vertebrate is a human.

49. A method according to any of the preceding claims,
wherein the vertebrate is a horse.

50. A method according to any of the preceding claims,
20   wherein the vertebrate is a large ape, a great ape or an
anthropoid ape.

51. A method according to any of the preceding claims,
wherein the vertebrate is a pig.

52. A method according to any of the preceding claims,
25   wherein the vertebrate is a cow.

53. A method according to any of the preceding claims,
wherein the bone is taken from the group consisting of
radius, femur, corpus vertebrae (L1, L2, L3, L4, L5, T1, T2,
T3, T4, T5, T6, T7, T8, T9, T10, T11, T12, C1, C2, C3, C4,
30   C5, C6, C7), calcaneus, talus, os carpi, metatars, metacarpi,

falanges, tibia, fibula, patella, ulna, humerus, mandible,
clavicula, scapula, os coxae, os naviculare, os cuboideum, os
cuneiform I, os cuneiform II, os cuneiform III, os sacrum, os
coccygis.

5 54. A method for estimating the bone quality of a vertebrate,
on the basis of two-dimensional image data comprising
information relating to the trabecular structure of at least
a part of a bone of the vertebrate, the image data being data
obtained by exposing at least the part of the bone to
10 electromagnetic radiation, the method comprising subjecting
the image data to a statistical analysis comprising

-   a background correction procedure in which low frequent
    intensity variations not related to the trabecular
    structure of the bone is reduced relative to image data
15   related to the trabecular structure of the part of the
    bone,
-   an image manipulation and feature extraction procedure
    comprising subjecting the image data to at least one of
    the following procedures:
20   (a)   obtaining an estimate of the parametric estimate
            of the power spectrum of the image data and
            extracting features relating to the energy
            distribution of the parametric estimate,
    (b)   obtaining, on the basis of image data on which a
25   Fourier method has been used to emphasize the
            information in the image data relating to the
            trabecular structure, an estimate of a grey-level
            co-occurrence matrix and extracting at least one
            feature on the basis of the estimated co-
30   occurrence matrix,
    (c)   obtaining an estimate of the projected trabecular
            pattern of the image data by using a Fourier
            method to emphasize the information in the image
            data relating to the trabecular structure and
35   subjecting the manipulated image data to a
            morphological operation, and extracting features

relating to the trabecular structure from the
estimated projected trabecular pattern,

(d)   obtaining, on the basis of a frequency analysis
of the image data, features relating to the
5   periodicity of the trabecular structure of the
part of the bone,

-    and an estimation procedure in which the bone quality of
the vertebrate is estimated with a Multiple Correlation
Coefficient better than 0.5 on the basis of the derived
10   features and optionally other features related to the
bone or the vertebrate and a predetermined relationship
between the features and reference bone quality
parameters.

55. A method according to claim 54, wherein the bone quality
15 of the vertebrate is estimated with a Multiple Correlation
Coefficient better than 0.55, such as better than 0.6,
preferably better than 0.65, such as better than 0.7,
preferably better than 0.8, such as better than 0.85.

56. A method for estimating Non-Causal Simultaneous Auto-
20 Regressive Moving Average models in two or more dimensions,
the method comprising optimizing a given direct measure of
the flatness of the residual spectrum of the model.

57. A method according to claim 56, wherein the optimization
of the given flatness measure is obtained by
25 (a) generating a set of initial parameters for the model,
(b) generating the residual spectrum of the model on the
basis of the parameters,
(c) obtaining the measure of the flatness of the residual
spectrum,
30 (d) obtaining a new iterate of the parameters on the basis
of the flatness measure and a search direction in
parameter space,
(e) repeating steps (b)-(d) until given stop criterion is
reached.

58. A method according to claims 56 or 57, wherein the
measure of flatness of the residual spectrum is obtained as
the entropy of the normalized residual power spectrum, dis-
regarding the DC value.

80
AMENDED CLAIMS
[received by the International Bureau on 13 February 1996 (13.02.96);
original claims 1-58 replaced by
amended claims 1-60 (12 pages)]

1. A method for estimating the bone quality of a vertebrate,
on the basis of two-dimensional image data comprising infor-
mation relating to the trabecular structure of at least a
5   part of a bone of the vertebrate, the image data being data
obtained by exposing at least the part of the bone to elec-
tromagnetic radiation, the method comprising subjecting the
image data to a statistical analysis comprising

-    a background correction procedure in which low frequent
10   intensity variations not related to the trabecular struc-
ture of the bone is reduced relative to image data
related to the trabecular structure of the part of the
bone,
-    an image manipulation and feature extraction procedure
15   wherein at least the local image intensity information as
well as variation in the local intensity are utilized to
extract information related to the trabecular structure
of the part of the bone, the image manipulation and fea-
ture extraction procedure comprising subjecting the image
20   data to at least one of the following procedures:
(a)   obtaining an estimate of the parametric estimate
of the power spectrum of the image data and
extracting features relating to the energy
distribution of the parametric estimate,
25   (b)   obtaining, on the basis of image data on which a
Fourier method has been used to emphasize the
information in the image data relating to the
trabecular structure, an estimate of a grey-level
co-occurrence matrix and extracting at least one
30   feature on the basis of the estimated co-
occurrence matrix,
(c)   obtaining an estimate of the projected trabecular
pattern of the image data by using a Fourier
method to emphasize the information in the image
35   data relating to the trabecular structure and
subjecting the manipulated image data to a

AMENDED SHEET (ARTICLE 19)

morphological operation, and extracting features
relating to the trabecular structure from the
estimated projected trabecular pattern,

(d)   obtaining, on the basis of a frequency analysis
5   of the power spectrum of the image data, a
        smoothed periodogram of the image data, or an
        estimate of the parametric estimate of the power
        spectrum of the image data, features relating to
        the periodicity of the trabecular structure of
10   the part of the bone,

 -     and an estimation procedure in which the bone quality of
       the vertebrate is estimated on the basis of the derived
       features and optionally other features related to the
       bone or the vertebrate and a predetermined relationship
15   between the features and reference bone quality parame-
       ters.

2. A method according to claim 1, wherein the electromagnetic
radiation is X-ray radiation.

3. A method according to any of the preceding claims, wherein
20 the image data is scanned from an X-ray film.

4. A method according to claim 3, wherein the resolution of
the X-ray film is at least 4 pairs of lines per centimetre,
such as at least 5 pairs of lines per centimetre.

5. A method according to claim 4, wherein the resolution of
25 the X-ray film is at least 10 pairs of lines per centimetre,
such as at least 25 pairs of lines per centimetre, preferably
at least 50 pairs of lines per centimetre.

6. A method according to claim 5, wherein the resolution of
the X-ray film is at least 100 pairs of lines per centimetre,
30 such as at least 250 pairs of lines per centimetre, preferab-
ly at least 500 pairs of lines per centimetre, such as at
least 600 pairs of lines per centimetre.

7. A method according to claim 3, wherein the scanning has been performed at a resolution of at least 10 lines per cm.

8. A method according to claim 7, wherein the resolution is at least 25 lines per cm.

5   9. A method according to claim 8, wherein the resolution is at least 100 lines per cm, such as at least 200 lines per cm, such as at least 250 lines per cm.

10. A method according to any of the preceding claims, where-in the background correction procedure comprises at least
10 reducing or optionally removing low frequency information having a frequency significantly lower than the spacing of the projected trabeculae.

11. A method according to claim 10, wherein information having frequencies half or less than the spacing of the
15 projected trabeculae is at least reduced or optionally removed.

12. A method according to claim 11, wherein information having frequencies being a quarter or less than the spacing of the projected trabeculae is at least reduced or optionally
20 removed.

13. A method according to claim 12, wherein information having frequencies being a tenth or less the spacing of the projected trabeculae is at least reduced or optionally removed.

25 14. A method according to any of claims 10-13, wherein the background correction procedure comprises generating second-ary image d ..a as a result of performing a median filtering with a pr . termined kernel size and subtracting this result from the   ginal image data.

15. A method according to any of claims 10-13, wherein the background correction procedure comprises generating secondary image data as a result of performing a mean filtering with a predetermined kernel size and subtracting this result

5   from the original image data.

16. A method according to any of claims 10-13, wherein the background correction procedure comprises globally fitting a two-dimensional polynomial to the image data and generating background corrected image data on the basis of the residuals

10   of the fitting procedure.

17. A method according to claim 16, wherein the order of the polynomial is at the most 15, such as at the most 10, preferably at the most 5.

18. A method according to claim 14 or 15, wherein the kernel

15   size is at the most 1/2 of the image data, such as at the most 1/4 of the image data, preferably at the most 1/10 of the image data, more preferably at the most 1/20 of the image data.

19. A method according to any of the preceding claims, where-

20   in the parametric estimate of the power spectrum is estimated by using a method selected from the group consisting of direct methods, auto-covariance methods and parametric methods.

20. A method according to claim 19, wherein the image data,

25   optionally weighted with a window, is subjected to a Fast Fourier Transformation in order to generate the parametric estimate.

21. A method according to claim 19, wherein the auto-covariance function estimated on the basis of the image data,

30   optionally weighted with a window, is subjected to a Fast Fourier Transformation in order to generate the parametric estimate.

22. A method according to claim 19, wherein one of the
methods on the basis of which the parametric estimate is
obtained is chosen from the group consisting of: causal
Simultaneous Auto-Regressive Moving Average (SARMA) models,
5   non-causal SARMA models, Gaussian Markov Random Field models
and Maximum Entropy Spectral Estimates and wherein the order
of the model is identified, the parameters of the model are
estimated and the spectrum of the estimated model is gener-
ated.

10   23. A method according to claim 22, wherein the method on the
basis of which the parametric estimate is obtained, is a non-
causal SARMA model using an estimator according to claim 58.

24. A method according to any of the preceding claims, where-
in at least one feature is related to parameters of a contour
15   encompassing at least a predetermined percentage of the
energy of the power spectrum.

25. A method according to claim 24, wherein the contour is
determined by
   (a)   defining a contour, in terms of one axes in each
20   dimension, around the centre of the power spectrum,
            all points on the contour having substantially the
            same distance to the centre of the power spectrum,
            and the contour encompassing less than the predeter-
            mined percentage of the energy of the power spectrum,
25   (b)   for each dimension of the data calculating the per-
            centage of the energy of the power spectrum
            encompassed by a dilated contour in which the axis in
            the dimension in question is increased by a predeter-
            mined distance,
30   (c)   increasing the axis of the contour, in the dimension
            in which the increase in energy encompassed by the
            dilated contour is the largest, by the predetermined
            distance and

(d)   repeating steps (b) and (c) until the percentage
         encompassed by the contour exceeds or equals the
         predetermined percentage.

26. A method according to claim 24 or 25, wherein the contour
-5 is ellipsoidal, optionally spherical.

27. A method according to claim 25 or 26, wherein the axis of
the contour are orthogonal and are defined along principal
directions of the power spectrum.

28. A method according to claim 1, wherein procedure (c) is
10 used and wherein the Fourier method comprises
   -   subjecting the image data to Fourier transformation,
   -   performing a subsequent mathematical transformation of
       the Fourier transformed data,
   -   converting the transformed data back into the spatial
15   domain.

29. A method according to claim 28, wherein the subsequent
mathematical transformation is linear or non-linear.

30. A method according to claim 29, wherein the subsequent
mathematical transformation is performed by raising the data
20 to a power larger than 1, such as a power in the range of
1.1-10, preferably 1.5-4, such as about 2.0.

31. A method according to any of claims 28-30, wherein a
third mathematical transformation is performed in order to
preserve only part of the magnitude information of the trans-
25 formed data.

32. A method according to any of claims 28-31, wherein the
emphasized information in the image data relating to the
trabecular structure is subjected to a grey-scale morphologi-
cal operation.

33. A method according to claim 32, wherein the grey-scale morphological operation is a top-hat operation wherein all pixels fitting in the top-hat are assigned a value different from a specified background pixel value.

5   34. A method according to claim 33, wherein the image data which has been subjected to the top-hat operation is thresholded so as to assign a foreground pixel value to the pixels having a pixel value different from the background pixel value.

10   35. A method according to any of claims 32-34, wherein the image data which has been subjected to the grey-scale morphological operation is subjected to further noise reduction to substantially remove isolated single pixels and pixel groups smaller than a predetermined threshold number of 15   pixels having a pixel value different from the background pixel value.

36. A method according to any of claims 32-35, wherein an operation is performed comprising determining, for each background pixel, the distance according to a given metric 20   from the background pixel to the nearest foreground pixel, and wherein at least one feature is extracted from the result of the operation.

37. A method according to claim 36, wherein at least one feature relates to a mean value and/or standard deviation 25   and/or the coefficient of variation and/or skewness and/or kurtosis of the determined distances from all background pixels to the nearest foreground pixel.

38. A method according to any of claims 32-35, wherein an operation is performed comprising determining a measure for 30   each background pixel based upon determining the distance from the background pixel in a number of given directions in the image data to the nearest foreground pixel and at least one feature is extracted from the result of the operation.

AMENDED SHEET (ARTICLE 19)

39. A method according to claim 38, wherein at least one feature relates to a mean value and/or standard deviation and/or the coefficient of variation and/or skewness and/or kurtosis of the determined measures for all background
5   pixels.

40. A method according to claim 38 or 39, wherein the measure for each background pixel is a mean value and/or standard deviation and/or the coefficient of variation and/or skewness and/or kurtosis and/or maximum distance of the determined
10 distances in the given directions.

41. A method according to any of the preceding claims, wherein at least one feature related to the bone or to the vertebrate, such as age and/or sex, and/or species, and/or race and/or the specific bone considered in the vertebrate,
15 and/or an estimated Bone Mineral Density of the bone, and/or an estimated Bone Mineral Content of the bone, is included in the estimation procedure.

42. A method according to claim 41, wherein the Bone Mineral Density is estimated by including data from a reference
20 object in the exposure of the bone to the electromagnetic radiation and where the Bone Mineral Density is estimated by correlating the absorption of the electromagnetic radiation of the bone and of the reference object.

43. A method according to any of the preceding claims,
25 wherein the estimation procedure is based on a statistical model, taking into account the correlation structure in the data set, so as to assign appropriate weights to the significant features in accordance with the predetermined relationship.

30 44. A method according to any of the preceding claims, wherein the reference bone quality is an absolute or relative bone quality of bones for which image data have been processed in accordance with any of the preceding claims.

45. A method according to claim 44, wherein the reference bone quality is determined on the basis of measurement of the mechanical bone strength, and/or Bone Mineral Density measurement, and/or on the basis of a Bone Mineral Content

5   measurement, and/or on the basis of a score of the bone strength by a skilled radiologist.

46. A method according to any of the preceding claims, wherein the predetermined relationship between the features and reference bone quality parameters is established on the

10   basis of reference bone quality parameters and features extracted according to any of the preceding claims.

47. A method according to claim 46, wherein the predetermined relationship is defined in terms of a model taken from the group consisting of: a General Linear Model, a Generalized

15   Linear Model, an Artificial Neural Network, a Causal Probabilistic Net and Classification And Regression Trees.

48. A method according to any of the preceding claims, wherein the vertebrate is a human.

49. A method according to any of the preceding claims,

20   wherein the vertebrate is a horse.

50. A method according to any of the preceding claims, wherein the vertebrate is a large ape, a great ape or an anthropoid ape.

51. A method according to any of the preceding claims,

25   wherein the vertebrate is a pig.

52. A method according to any of the preceding claims, wherein the vertebrate is a cow.

53. A method according to any of the preceding claims, wherein the bone is taken from the group consisting of

30   radius, femur, corpus vertebrae (L1, L2, L3, L4, L5, T1, T2,

T3, T4, T5, T6, T7, T8, T9, T10, T11, T12, C1, C2, C3, C4,
C5, C6, C7), calcaneus, talus, os carpi, metatars, metacarpi,
falanges, tibia, fibula, patella, ulna, humerus, mandible,
clavicula, scapula, os coxae, os naviculare, os cuboideum, os
5 cuneiform I, os cuneiform II, os cuneiform III, os sacrum, os
coccygis.

54. A method according to claim 1, wherein procedure (d) is
used and wherein the features relating to the periodicity of
the trabecular structure of the part of the bone are derived
10 from information relating to the height, width and/or
curvature of peaks of and/or to the total area under peaks of
the power spectrum of the image data, the smoothed
periodogram of the image data, or the estimate of the
parametric estimate of the power spectrum of the image data.

15 55. A method according to claim 54, wherein the information
is derived relating to the height, width and/or curvature of
peaks of the smoothed periodogram of the image data and/or
total area under the peaks thereof, and wherein the position
of the peaks are identified in the power spectrum of the
20 image data.

56. A method for estimating the bone quality of a vertebrate,
on the basis of two-dimensional image data comprising
information relating to the trabecular structure of at least
a part of a bone of the vertebrate, the image data being data
25 obtained by exposing at least the part of the bone to
electromagnetic radiation, the method comprising subjecting
the image data to a statistical analysis comprising

-    a background correction procedure in which low frequent
     intensity variations not related to the trabecular
30   structure of the bone is reduced relative to image data
     related to the trabecular structure of the part of the
     bone,

-      an image manipulation and feature extraction procedure
       comprising subjecting the image data to at least one of
       the following procedures:

       (a)   obtaining an estimate of the parametric estimate
5   of the power spectrum of the image data and
                extracting features relating to the energy
                distribution of the parametric estimate,

       (b)   obtaining, on the basis of image data on which a
                Fourier method has been used to emphasize the
10   information in the image data relating to the
                trabecular structure, an estimate of a grey-level
                co-occurrence matrix and extracting at least one
                feature on the basis of the estimated co-
                occurrence matrix,

15   (c)   obtaining an estimate of the projected trabecular
                pattern of the image data by using a Fourier
                method to emphasize the information in the image
                data relating to the trabecular structure and
                subjecting the manipulated image data to a
20   morphological operation, and extracting features
                relating to the trabecular structure from the
                estimated projected trabecular pattern,

       (d)   obtaining, on the basis of a frequency analysis
                the power spectrum of the image data, a smoothed
25   periodogram of the image data, or a parametric
                estimate of the power spectrum of the image data,
                features relating to the periodicity of the
                trabecular structure of the part of the bone,

-      and an estimation procedure in which the bone quality of
30   the vertebrate is estimated with a Multiple Correlation
       Coefficient better than 0.5 on the basis of the derived
       features and optionally other features related to the
       bone or the vertebrate and a predetermined relationship
       between the features and reference bone quality
35   parameters.

57. A method according to claim 56, wherein the bone quality
of the vertebrate is estimated with a Multiple Correlation

Coefficient better than 0.55, such as better than 0.6, preferably better than 0.65, such as better than 0.7, preferably better than 0.8, such as better than 0.85.

58. A method for estimating Non-Causal Simultaneous Auto-
5   Regressive Moving Average models in two or more dimensions, the method comprising optimizing a given direct measure of the flatness of the residual spectrum of the model.

59. A method according to claim 58, wherein the optimization of the given flatness measure is obtained by
10   (a)   generating a set of initial parameters for the model,
     (b)   generating the residual spectrum of the model on the basis of the parameters,
     (c)   obtaining the measure of the flatness of the residual spectrum,
15   (d)   obtaining a new iterate of the parameters on the basis of the flatness measure and a search direction in parameter space,
     (e)   repeating steps (b)-(d) until given stop criterion is reached.

20   60. A method according to claims 58 or 5, wherein the measure of flatness of the residual spectrum is obtained as the entropy of the normalized residual power spectrum, disregarding the DC value.
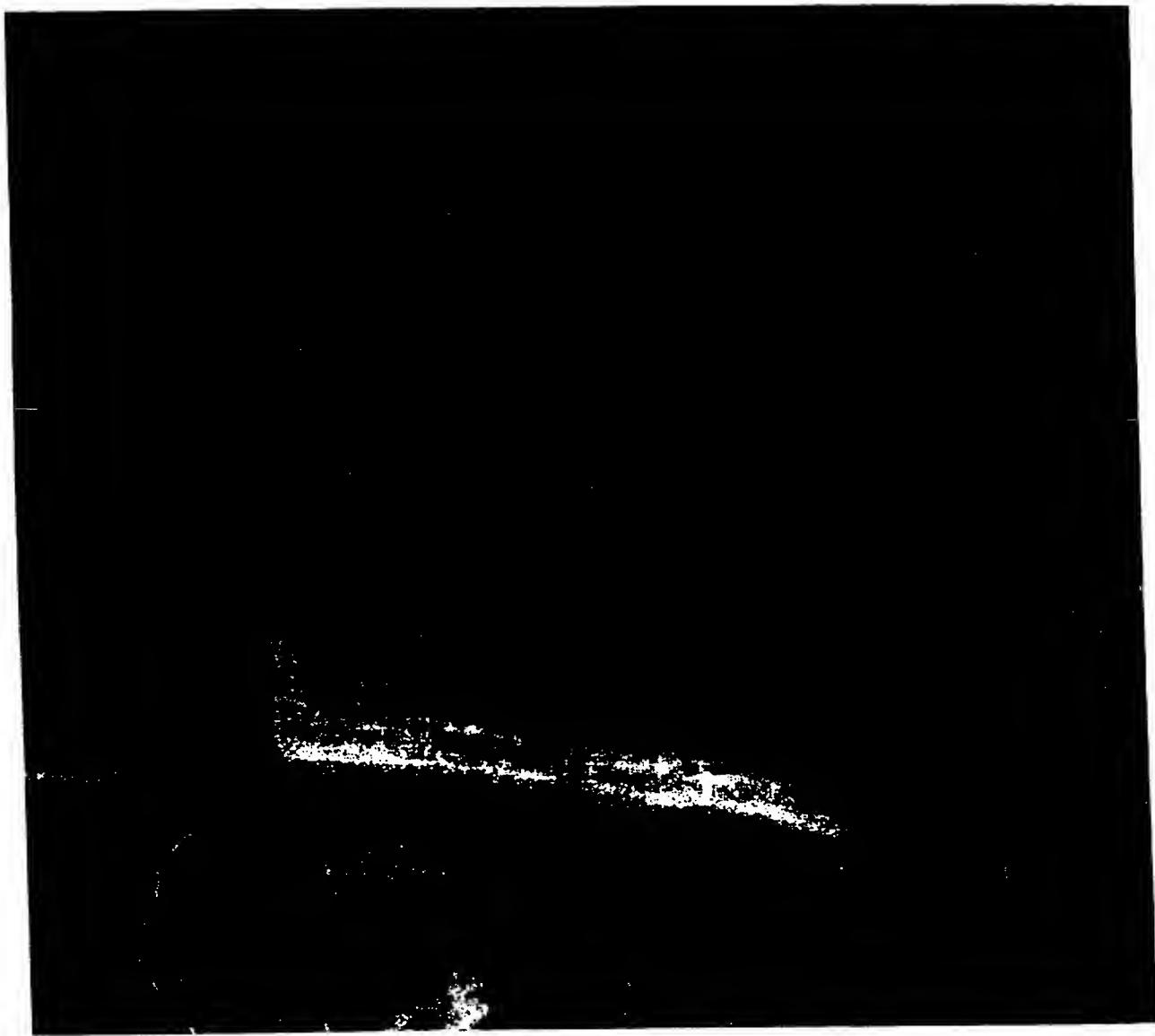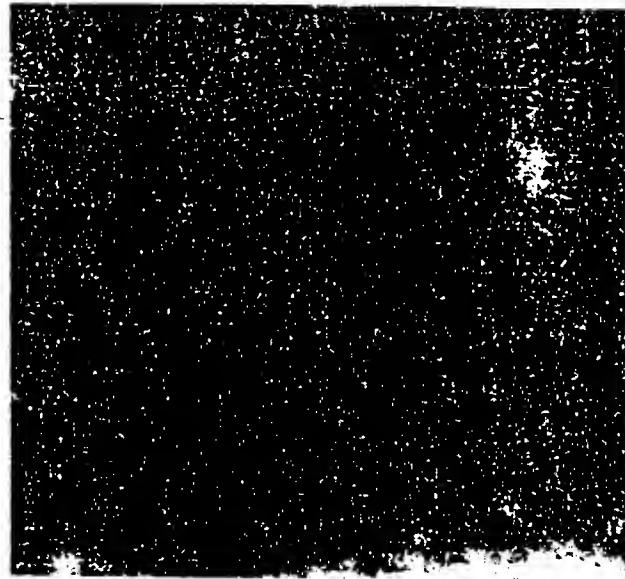
Fig. 1

Fig. 2
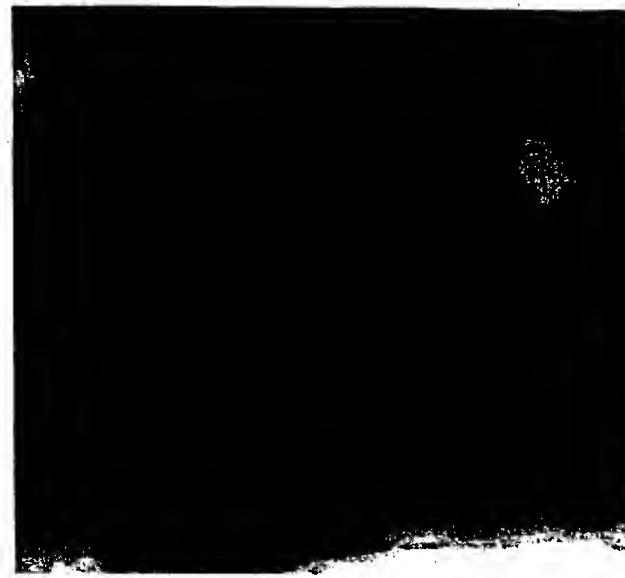
Fig. 3
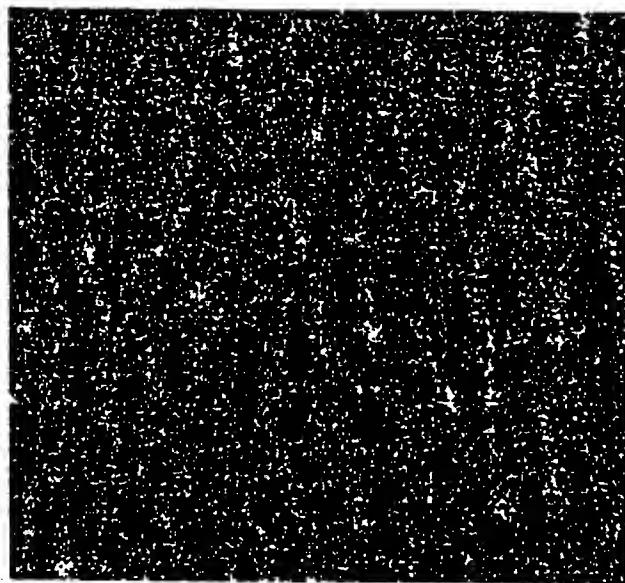
Fig. 4
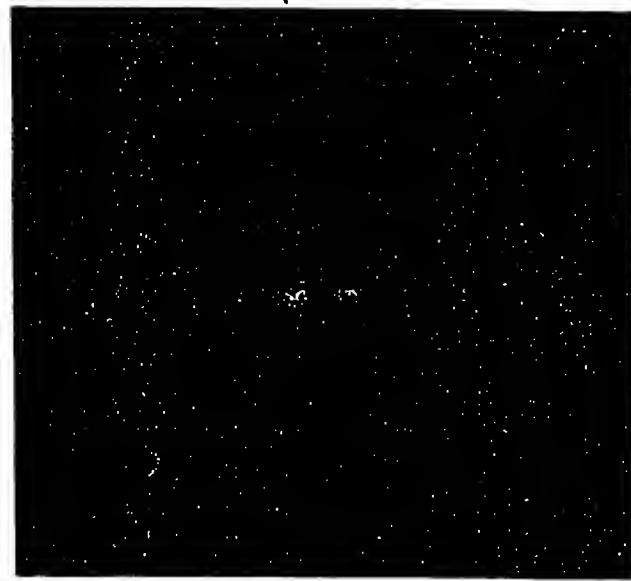
Fig. 5

Fig. 6

Fig. 7
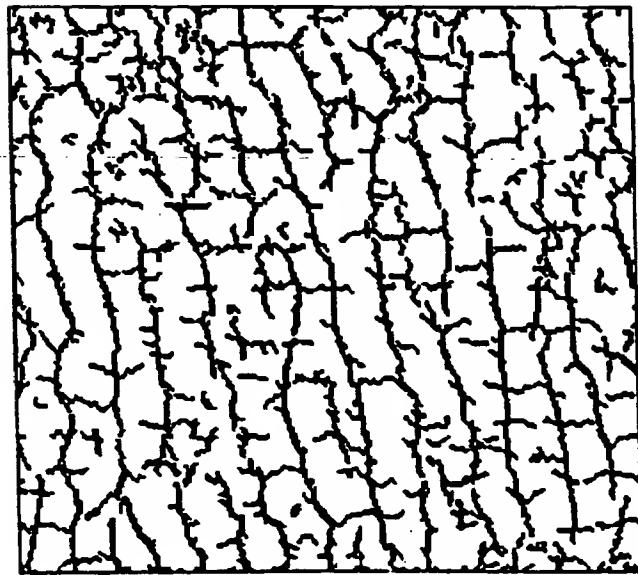
Fig. 8
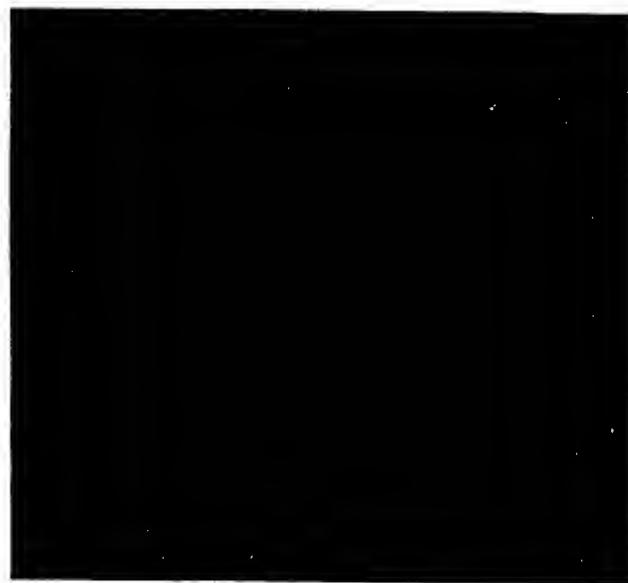
Fig. 9
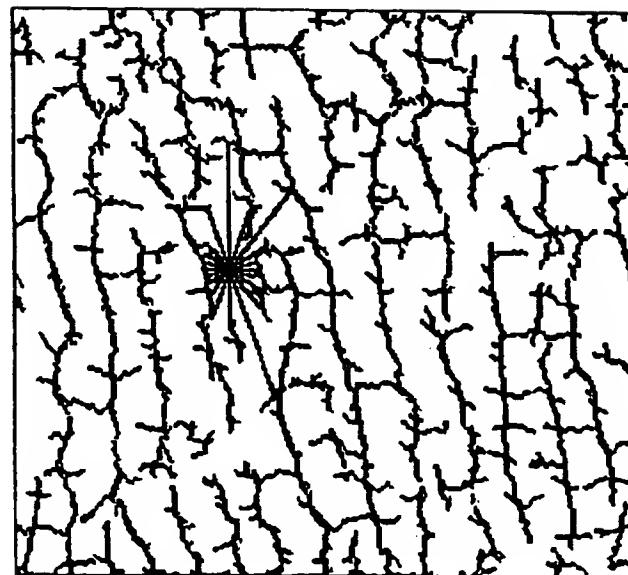
Fig. 10
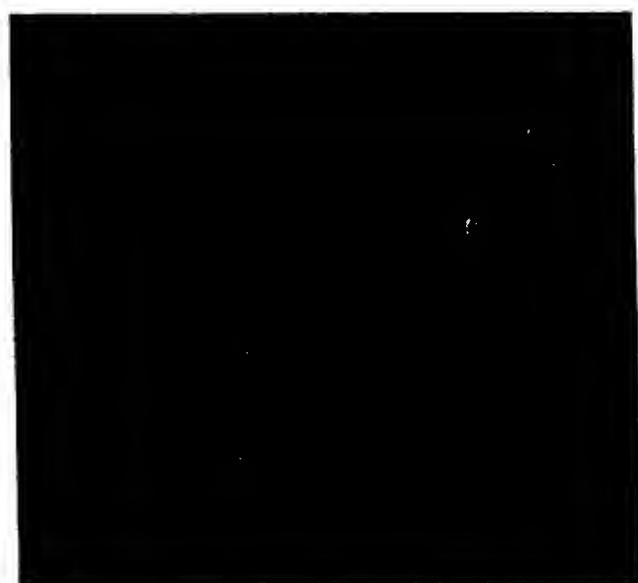
Fig. 11

Fig. 12
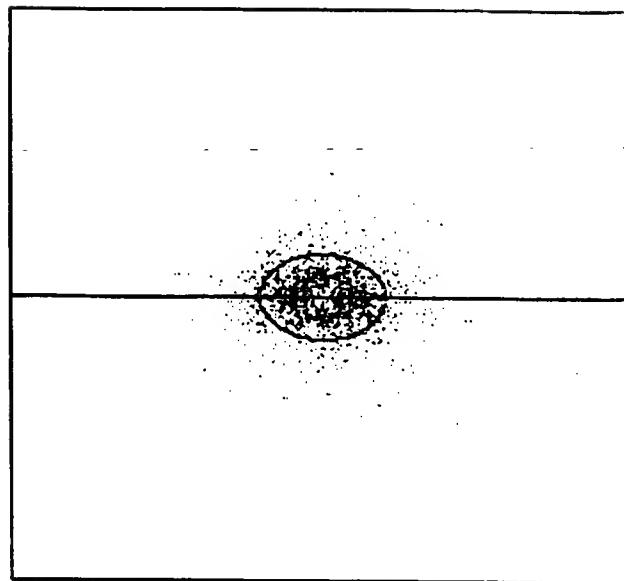
Fig. 13
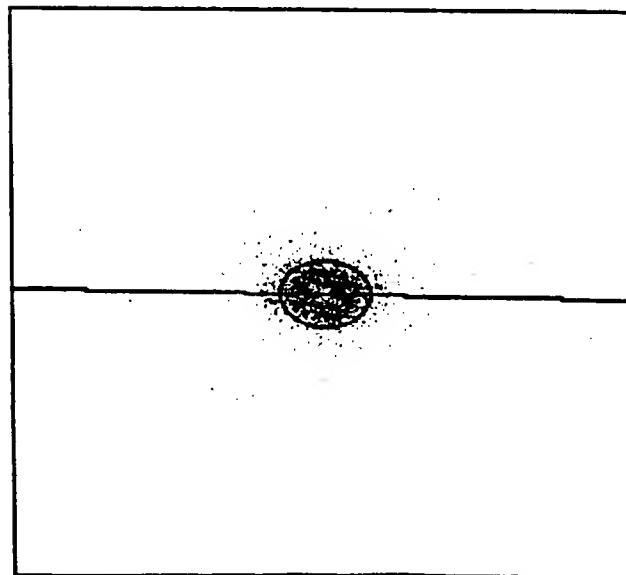
Fig. 14

LS estimates vs. true parameters (isotropic case)
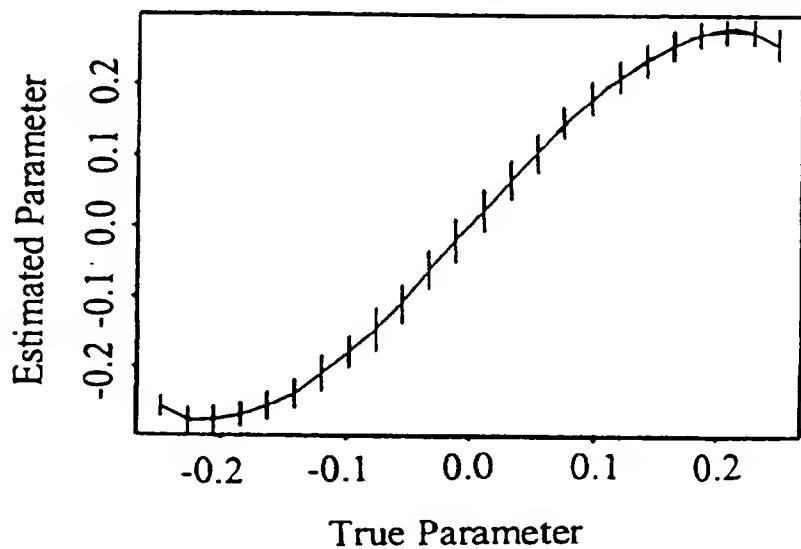
Fig. 15

Approx. ML estimates vs. true parameters (anisotropic case)

Fig. 16

Part of a Likelihood function
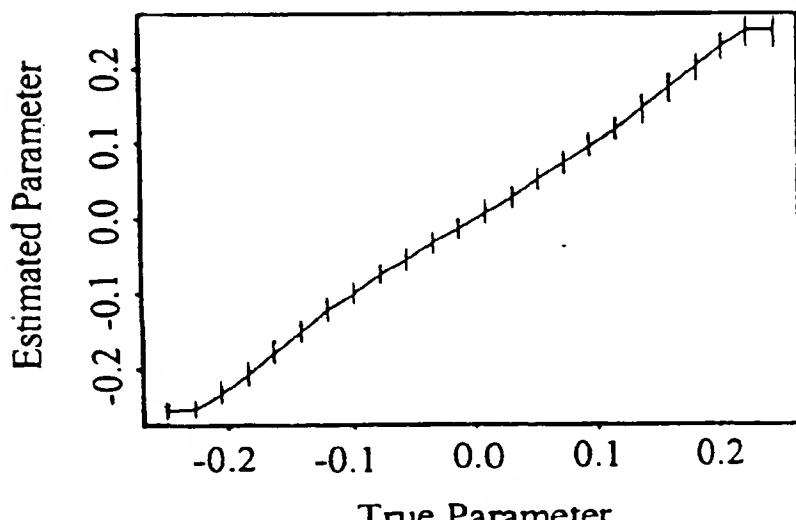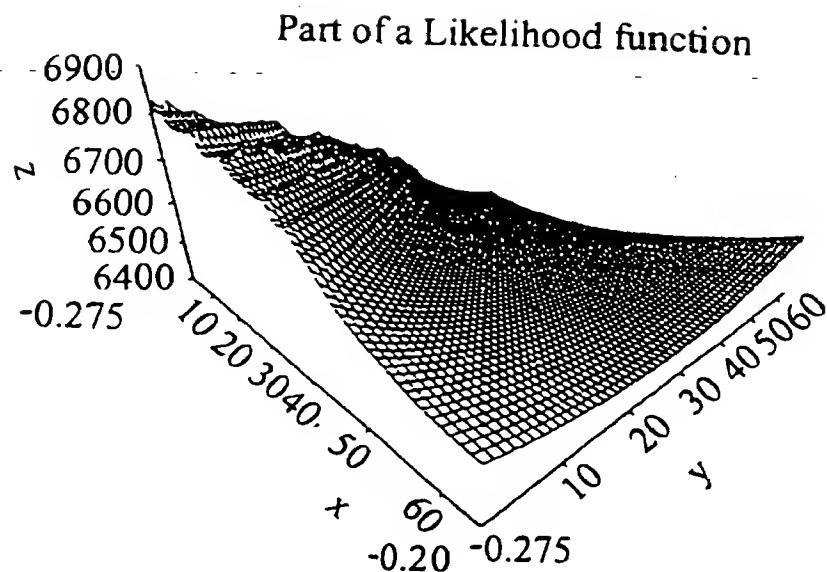
Fig. 17

Exact torus-ML estimates vs. true parameters (isotropic case)
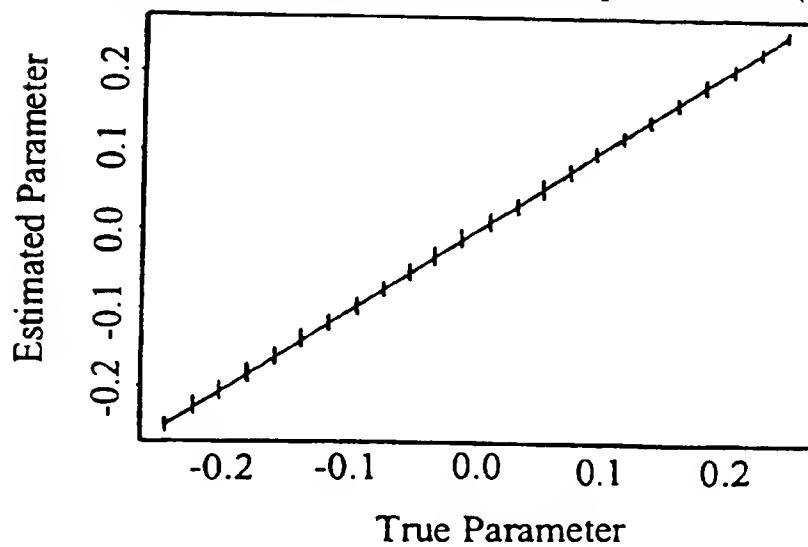
Fig. 18

MORSE estimates vs. true parameters (isotropic case)
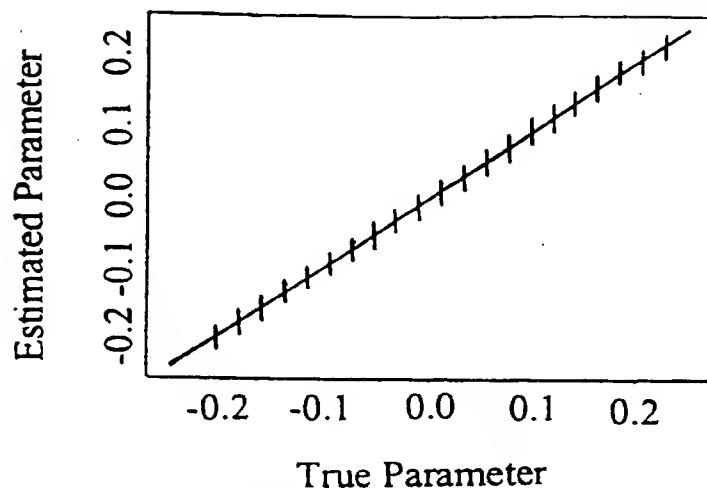
Fig. 19
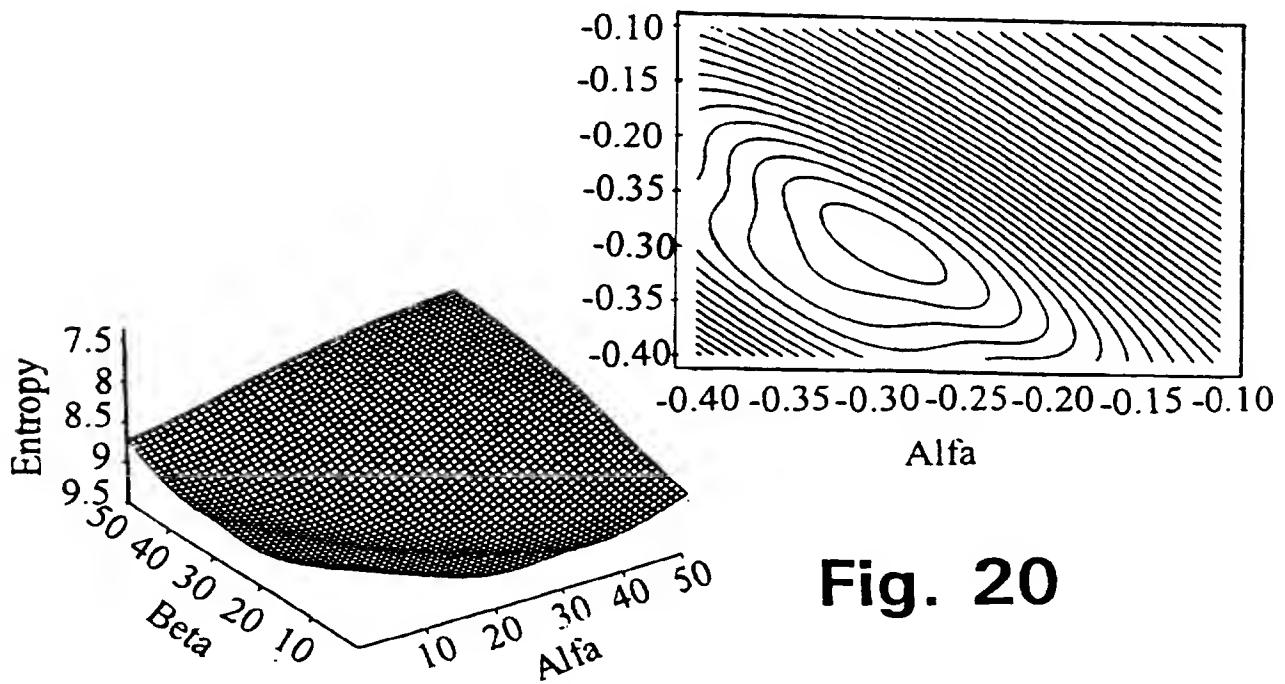
Fig. 20
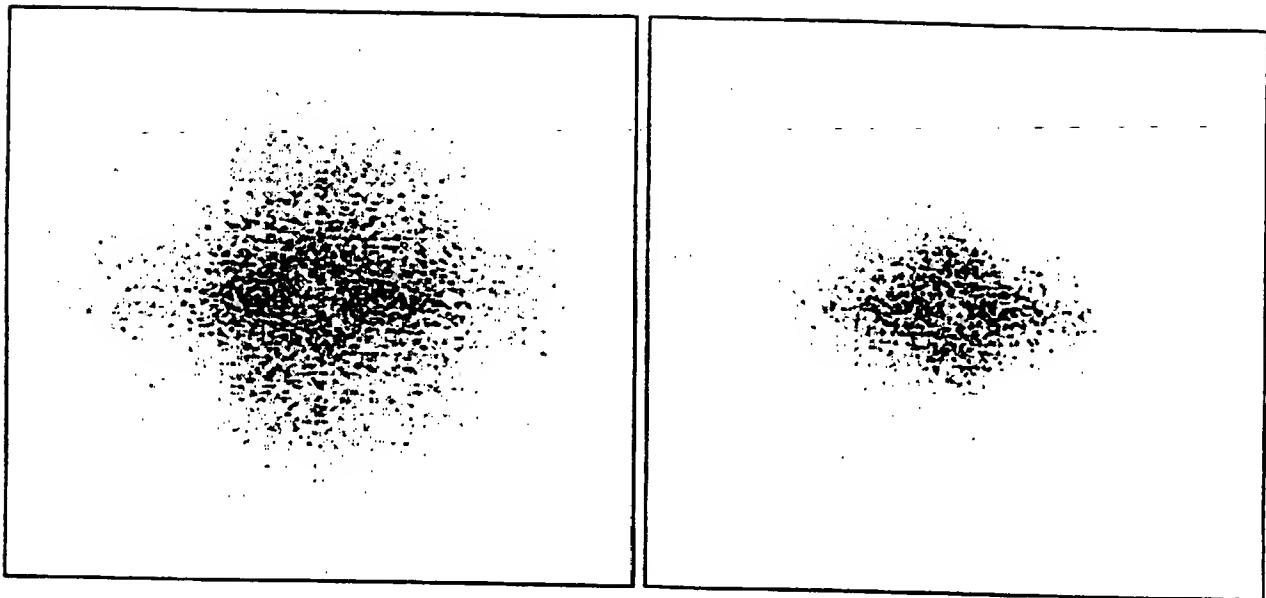
FIG. 21

FIG. 22

13/16

# FIG. 23

AR(0,-1)

AR((-1,0)

MA(0,-1)

MA(-1,0)
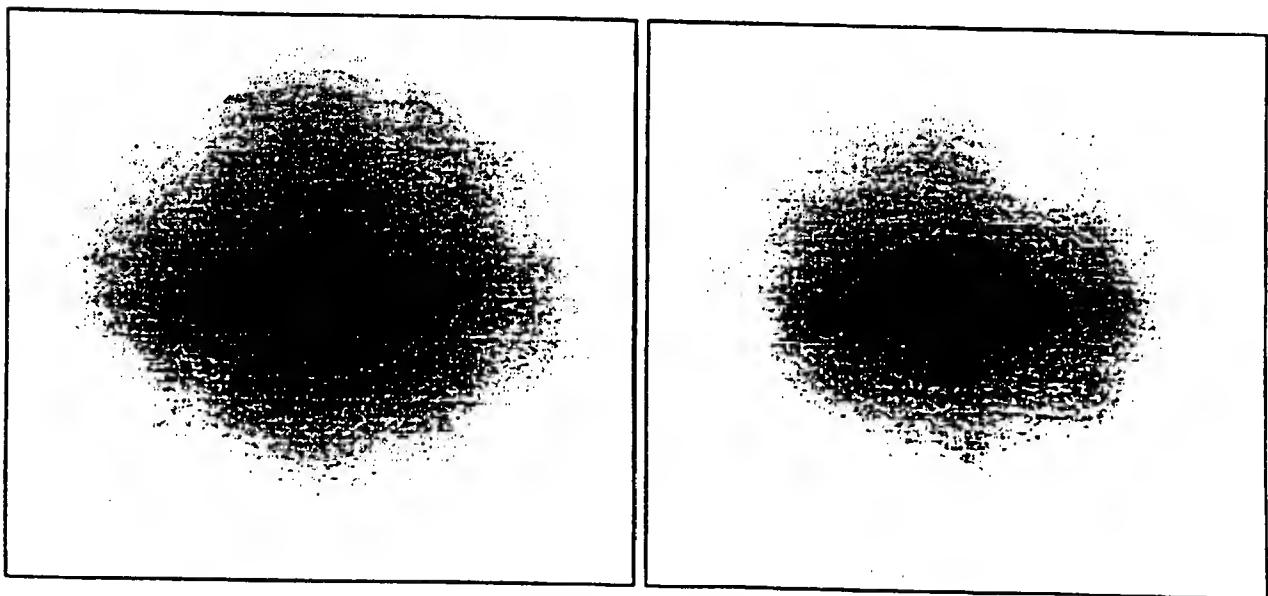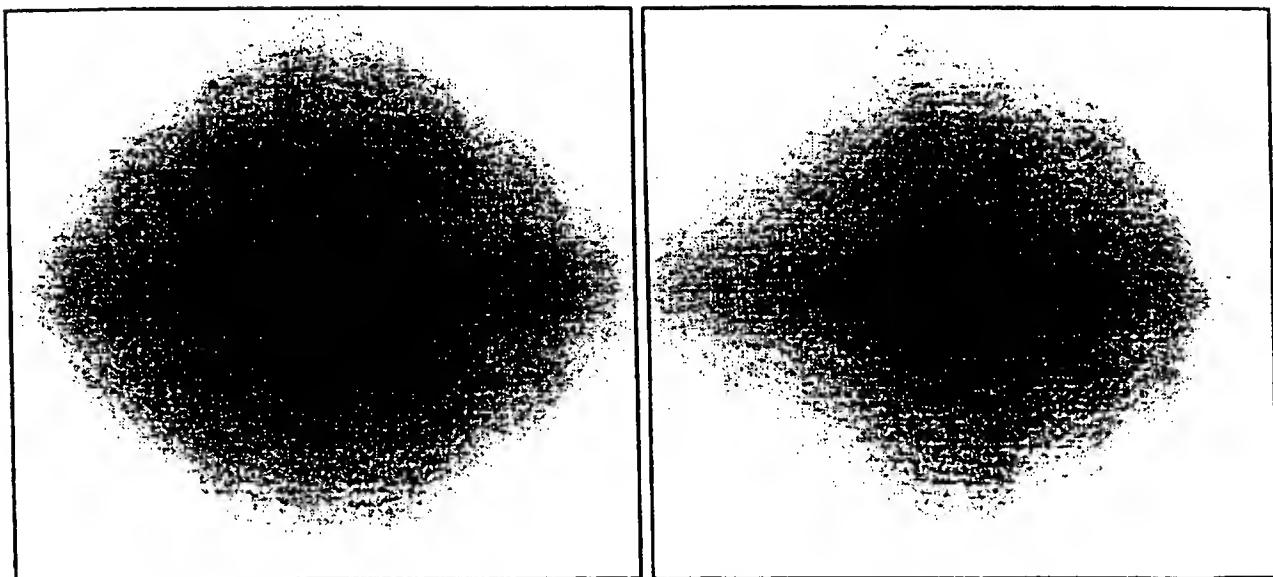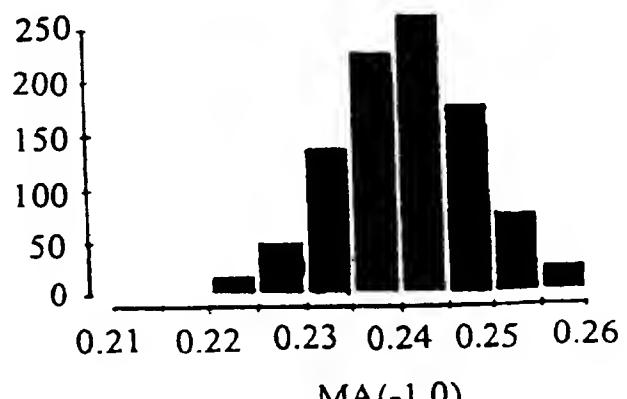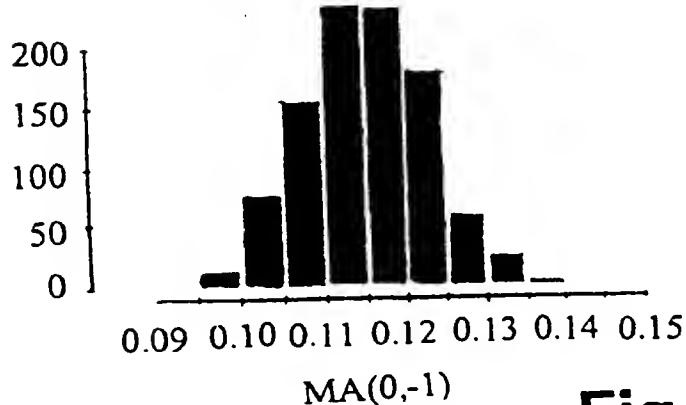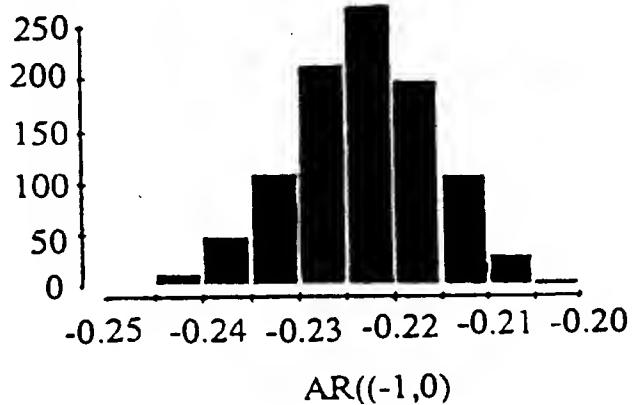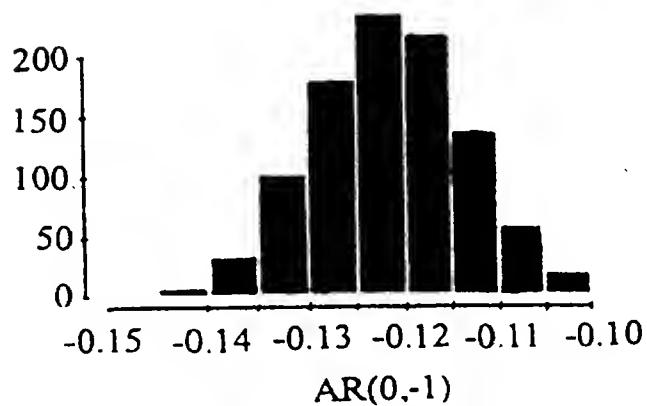
Fig. 25

14/16

| $\tau_i \in N$	θ_i	64 × 64 samples $\left[\bar{\theta}_i - \dfrac{2\hat{\sigma}_{\theta_i}}{\sqrt{1000}}; \bar{\theta}_i + \dfrac{2\hat{\sigma}_{\theta_i}}{\sqrt{1000}}\right]$	128 × 128 samples $\left[\bar{\theta}_i - \dfrac{2\hat{\sigma}_{\theta_i}}{\sqrt{1000}}; \bar{\theta}_i + \dfrac{2\hat{\sigma}_{\theta_i}}{\sqrt{1000}}\right]$
$AR(-1,0)$	-0.22314	[−0.22320; −0.22121]	[−0.22356; −0.22260]
$AR(0,-1)$	-0.12118	[−0.12232; −0.12024]	[−0.12178; −0.12075]
$MA(-1,0)$	0.11535	[0.11464; 0.11672]	[0.11473; 0.11570]
$MA(0,-1)$	0.24066	[0.23982; 0.24175]	[0.24035; 0.24131]

AR(0,-1)=-0.12118
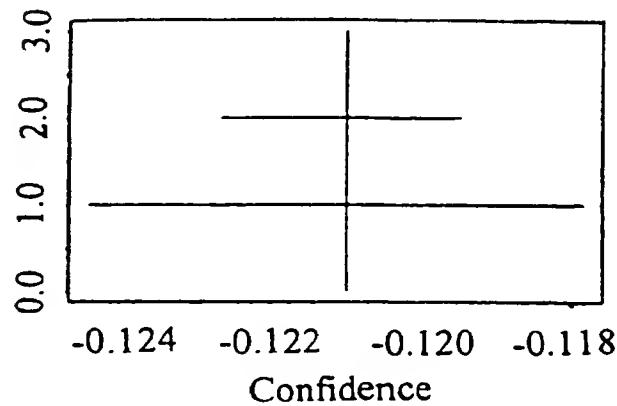
AR(-1,0)=-0.22314
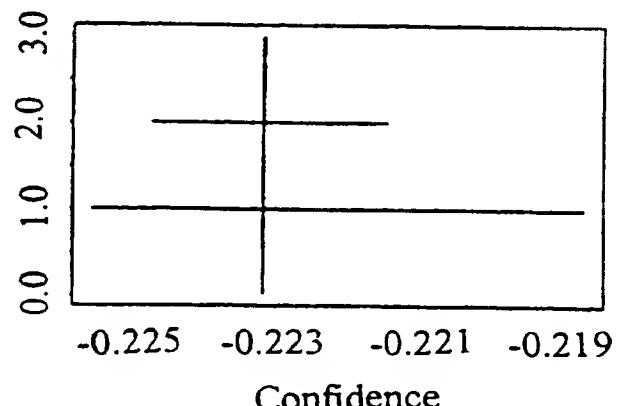
MA(-1,0)=0.11535

MA(0,-1)=0.24066

Fig. 24

Log(fracture load)

Multiple R-Squared = 0.816

predicted fracture load

Fig. 26

Log(fracture load)

Multiple R-Squared = 0.869

predicted fracture load
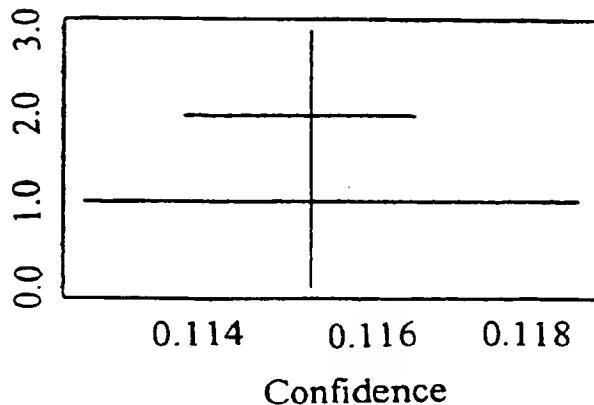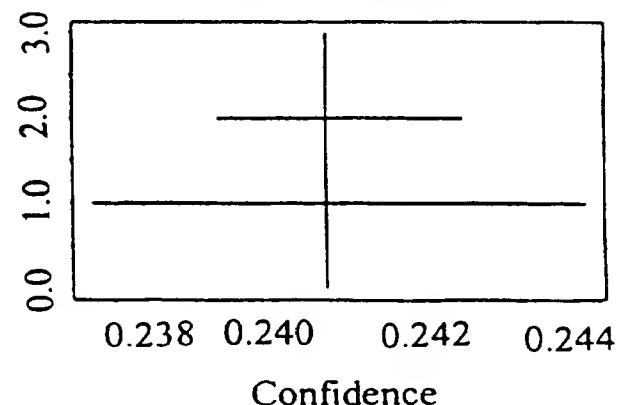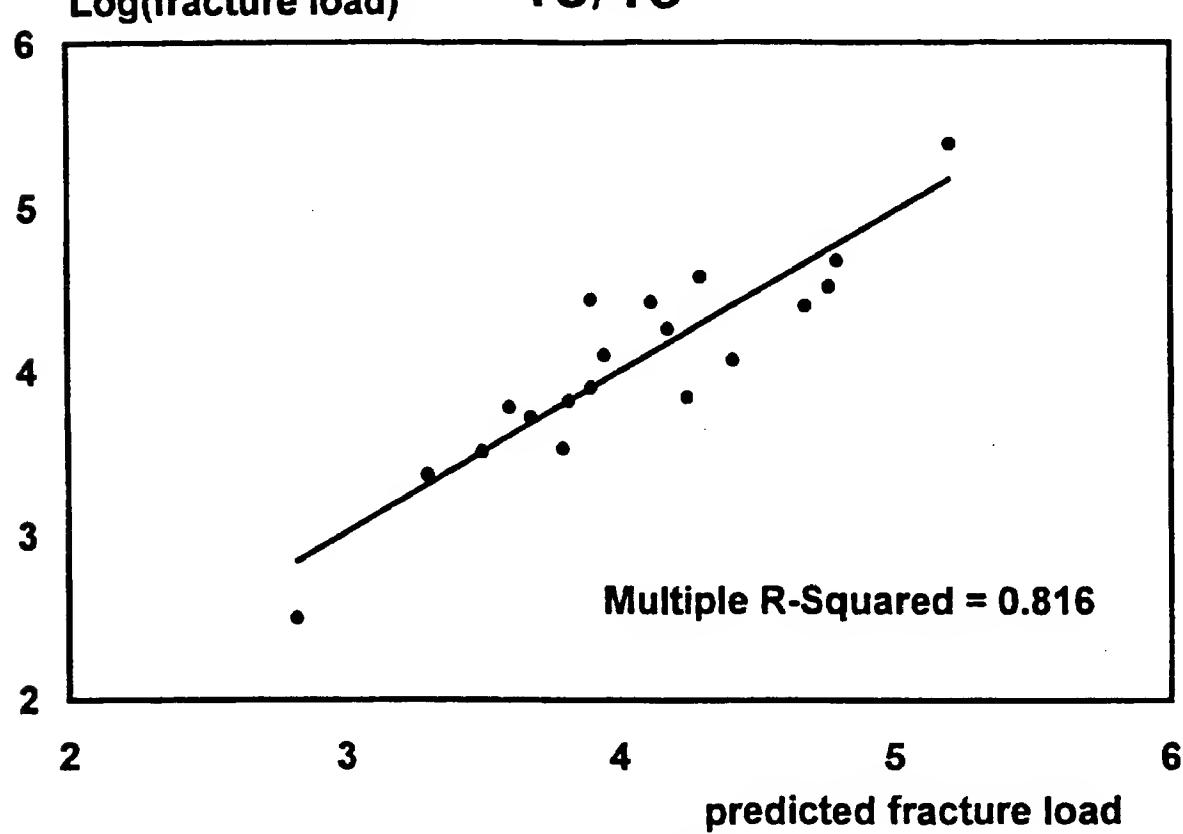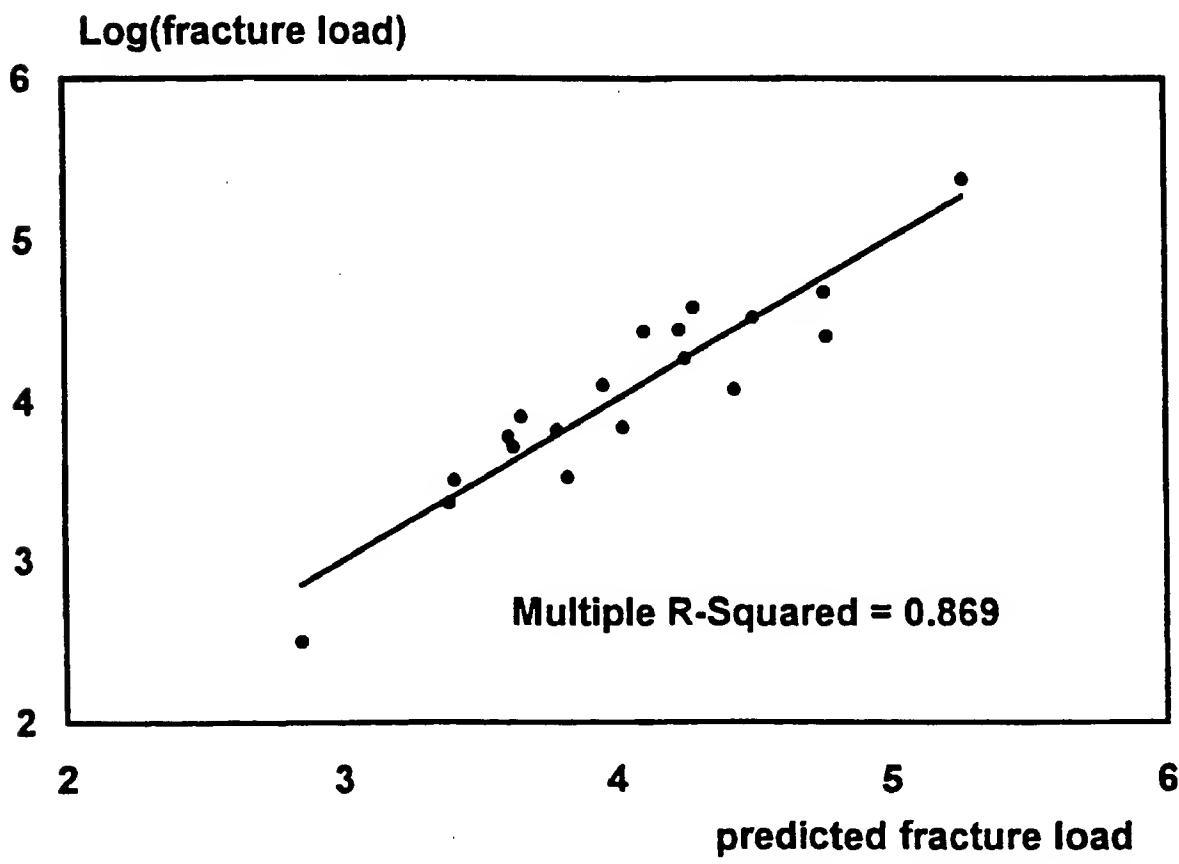
Fig. 27
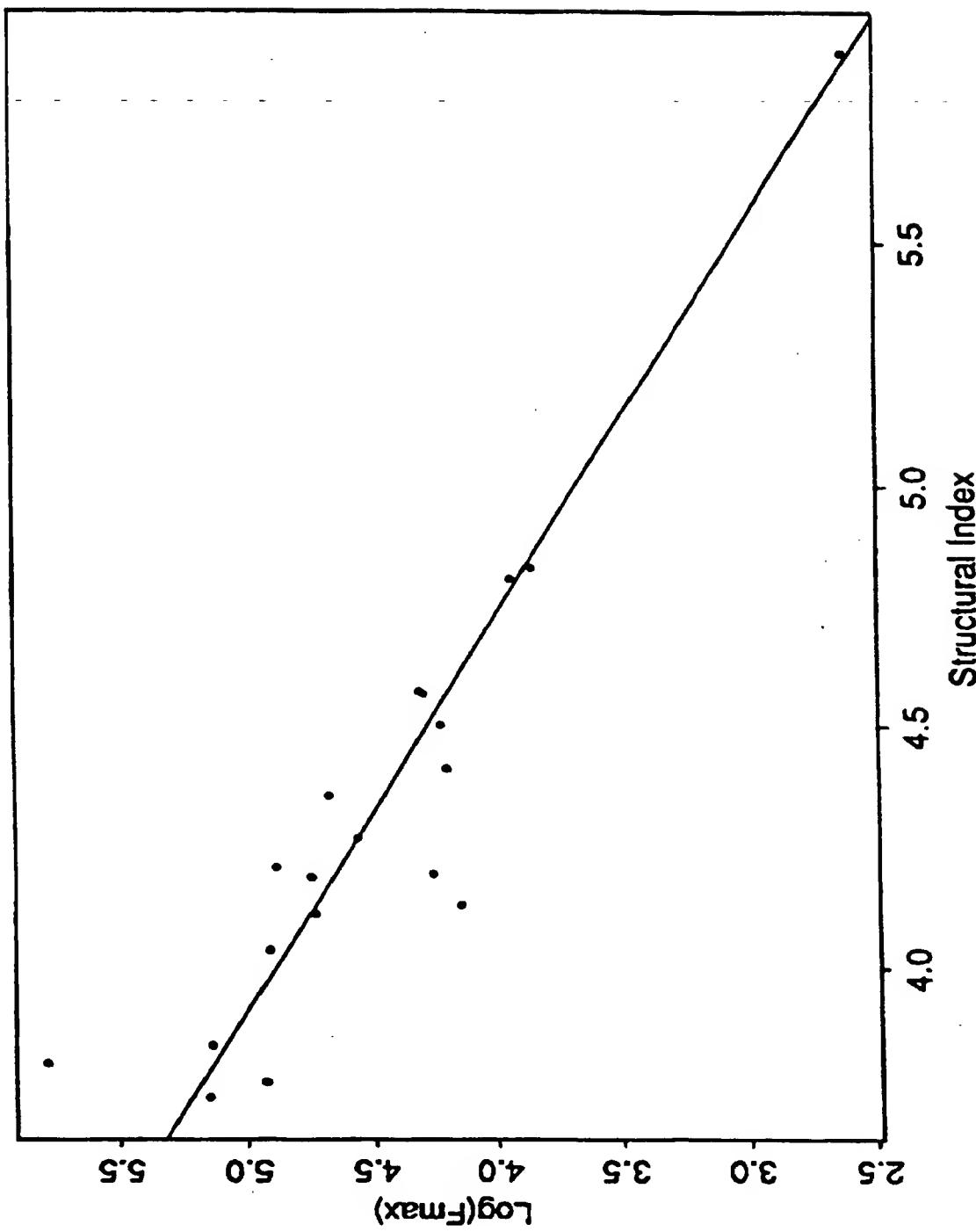
FIG. 28

B. FIELDS SEARCHED

Minimum documentation searched (classification system followed by classification symbols)

IPC 6   G06T

Documentation searched other than minimum documentation to the extent that such documents are included in the fields searched

Electronic data base consulted during the international search (name of data base and, where practical, search terms used)

C. DOCUMENTS CONSIDERED TO BE RELEVANT

Category*	Citation of document, with indication, where appropriate, of the relevant passages	Relevant to claim No.
X	MEDICAL PHYSICS, vol. 21, no. 8, August 1994 NEW YORK US, pages 1293-1300, XP 000466010 SHIRLEY N.C. CHENG ET AL. 'Automated segmentation of regions of interest on hand radiographs' see the whole document ---	1,54
X	MEDICAL PHYSICS, vol. 20, no. 4, August 1993 NEW YORK US, pages 983-992, XP 000388376 CHAIR-LI CHANG ET AL. 'Computer-aided diagnosis: Detection and characterization of hyperparathyroidism in digital hand radiographs' see the whole document --- -/--	1,54

[X] Further documents are listed in the continuation of box C.   [ ] Patent family members are listed in annex.

* Special categories of cited documents :

"A" document defining the general state of the art which is not considered to be of particular relevance

"E" earlier document but published on or after the international filing date

"L" document which may throw doubts on priority claim(s) or which is cited to establish the publication date of another citation or other special reason (as specified)

"O" document referring to an oral disclosure, use, exhibition or other means

"P" document published prior to the international filing date but later than the priority date claimed

"T" later document published after the international filing date or priority date and not in conflict with the application but cited to understand the principle or theory underlying the invention

"X" document of particular relevance; the claimed invention cannot be considered novel or cannot be considered to involve an inventive step when the document is taken alone

"Y" document of particular relevance; the claimed invention cannot be considered to involve an inventive step when the document is combined with one or more other such documents, such combination being obvious to a person skilled in the art.

"&" document member of the same patent family

Date of the actual completion of the international search	Date of mailing of the international search report
1 December 1995	2 1. 12. 95

Name and mailing address of the ISA	Authorized officer
European Patent Office, P.B. 5818 Patentlaan 2 NL - 2280 HV Rijswijk Tel. (+ 31-70) 340-2040, Tx. 31 651 epo nl, Fax (+ 31-70) 340-3016	Chateau, J-P

Form PCT/ISA/210 (second sheet) (July 1992)

2

page 1 of 2

Inter   nal Application No

PCT/DK 95/00338

C.(Continuation) DOCUMENTS CONSIDERED TO BE RELEVANT

Category*	Citation of document, with indication, where appropriate, of the relevant passages	Relevant to claim No.
A	PROCEEDINGS OF THE TWENTIETH ASILOMAR CONFERENCE ON SIGNALS,SYSTEMS AND COMPUTERS,NOVEMBER 10-12,1986 ,PACIFIC GROVE (US); IEEE COMPUTER SOCIETY PRESS, LOS ALAMITOS (US), pages 631-634, N. HAKIM ET AL. 'A digital image processing approach to diagnosis of osteoporosis' see the whole document ---	1,54
A	INTERNATIONAL JOURNAL OF BIO-MEDICAL COMPUTING, vol. 35, no. 2, March 1994 SHANNON IE, pages 141-153, XP 000434665 J.J. GOUGH ET AL. 'Variogram methods for the analysis of bony trabecular shadows in plain radiographs' see the whole document -----	1,54

2